DIFFUSION IN RARE-GAS LIQUIDS:

AN EXPERIMENTAL STUDY

A Thesis submitted for the Degree of

DOCTOR OF PHILOSOPHY

of

The Australian National University

by

KANDADAI SRINIVASAN

April 1981

DECLARATION

Except where acknowledgements are made in the text, the material contained in this thesis describes the original work of the candidate.

KANDADAI SRINIVASAN

ABSTRACT

This thesis describes the design and development of an apparatus for measuring the diffusion coefficients of cryogenic liquids. The diaphragm cell method is used. The experimental apparatus has a facility for the continuous monitoring of a radioactive tracer which is diffusing across a sintered stainless steel diaphragm. A scintillation counter assembly consisting of a cesium iodide crystal, a lucite light guide and a photomultiplier tube is used for this purpose. A temperature control method is incorporated which is capable of maintaining a set temperature to within ± 0.03 K in space and time.

Modified equations for the diaphragm cell are derived for the case of continuous monitoring. It is shown that neither the initial concentrations of the two compartments of the cell nor the exact starting time of diffusion are necessary to compute the diffusion coefficient.

The apparatus is used to measure the tracer diffusion coefficients of krypton in liquid argon over a temperature range of 85 - 103 K. The present data are discussed in relation to some other experimental and computer simulation results.

ACKNOWLEDGEMENTS

The author gratefully acknowledges the generous assistance rendered by so many people. The only reason for refraining from a detailed mention is that the list of names of persons and groups from whom the author has benefitted tends to be too lengthy. However, the author is duty bound to express his gratitude to:

Dr. R. Mills and Dr. L.A. Woolf - for suggesting the project, their supervision, constant encouragement and advice on the preparation of this thesis,

Mr. P.C. Scott and Mr. F.L. Wilson - for their superb workmanship in constructing the apparatus,

Mr. J. Altin and Mr. H.W. Heck - for designing the electronic systems of liquid nitrogen level controller and the thermal discriminator, and to

Miss B. Thangavadivel - for her overall assistance in bringing out this thesis.

TABLE OF CONTENTS

List of Figures

List of Photographic Plates

List of Tables

NOMENCLATURE

Symbol	Meaning	Equation
A	Constant (counts/min)	(3.5)
A_c	Effective cross-sectional area (cm^2)	(3.2)
B	Constant (counts/min)	(3.5)
b	Index governing the diffusion coefficient (s^{-1})	(3.5)
C	Counting rate (counts/min)	(3.1)
C_1	Mole fraction of argon	Figure 6.1
c_p	Specific heat (J/g-K)	(2.1)
D	Diffusion coefficient (cm^2/s)	(3.1)
ℓ	Effective thickness of diaphragm (cm)	(3.2)
m	Mass of the cell (g)	(2.1)
N	Number of data points	Appendix - I
P	Pressure (bar)	Table 5.1
Q	Heat transfer rate (W)	(2.1)
T	Temperature (K)	(2.1)
t	Time (s)	(3.1)
V	Volume (cm^3); Molar volume (cm^3/mole)	(3.2)
α	Coefficient of thermal contraction (K^{-1})	(3.10)
β	Cell constant (cm^{-2})	(3.1)
λ	$= 2V_D/(V_T+V_B)$	(3.2)
ρ	Density (g/cm^3)	Table 5.1

Subscripts: B - bottom compartment; D - diaphragm; T - top compartment; i - index of summation; Kr - krypton

Superscript: o - initial condition

1. INTRODUCTION

Of the three principal states of existence of matter, namely solid, liquid and gas, the liquid state is by far the least understood. The molecular structure in liquids seems to be indicative of a short range order and a long range disorder. Several theories have been put forward to explain the behaviour of liquids by considering them as either dense gases or quasi-crystalline solids. Reviews of the liquid state have been made by Mott (1952), Pryde (1966), Hansen and McDonald (1976), Watts and McGee (1976) and several other contributors.

Some understanding of the liquid state is possible through a study of either the equilibrium properties or the non-equilibrium transport properties, namely diffusion, viscosity and thermal conductivity. A theoretical treatment of the properties requires certain assumptions such as the form of the intermolecular potential and that the liquids are composed of spherical molecules which are chemically inert. Calculations based on fluid models or rigorous computer simulation of molecular motion can then be performed to evaluate the transport properties and at least in the latter case, the time dependent correlation functions which are related to the transport properties. In order to verify the validity of the theories, it is necessary to have relevant experimental evidence. The rare-gas liquids are the ones which are the closest to being 'simple liquids' because they are monoatomic, spherically symmetric and are chemically inert.

Table 1.1 gives a summary of the experimental investigations carried out so far to obtain diffusion coefficients in liquids argon and krypton . Experimental results pertaining to these two liquids have been chosen as more extensive studies were carried out on them compared to the others in the same family. Some typical

TABLE 1.1 : SUMMARY OF EXPERIMENTS ON DIFFUSION IN LIQUIDS ARGON AND KRYPTON

Diffusing species	Experimental investigators	Range		Method
		Temperature (K)	Pressure	
$Argon^{+}$ - Argon	Corbett and Wang (1956)	84.31	658 torr	Capillary cell
	Cini-Castagnoli and Ricci (1960)	84.5 to 90.1	2 atm	Capillary cell
	Naghizadeh and Rice (1962)	85.1 to 108	12.9 to 135 atm	Capillary cell
Argon - Argon	Dasannacharya and Rao (1965)	84.5		Neutron diffraction
	Zandveld et al (1970)	85.7 to 115.9		Neutron diffraction
$Krypton^{+}$ - Krypton	Naghizadeh and Rice (1962)	118.4 to 147.1	8.5 to 39.1 atm	Capillary cell
Krypton - Krypton	Cowgill and Norberg (1976)	116 to 200	along liquid-vapour co-existence curve	Nuclear magnetic resonance
$Krypton^{+}$ - Argon	Cini-Castagnoli and Ricci (1960)	85.4 to 90.2	2 atm	Capillary cell

+ - Tagged isotope

values are reproduced below for the sake of comparison.

TABLE 1.2 : SELF-DIFFUSION COEFFICIENTS IN LIQUIDS ARGON AND KRYPTON

Temperature (K)	Pressure (atm)	D x 10^5 (cm^2/s)	Method	Reference
		A. Liquid argon		
84.31	0.86	2.07±0.07	CC	Corbett and Wang(1956)
84.56	0.92	1.53±0.03	CC	Cini-Castagnoli and Ricci (1960)
85.10	12.9	1.84±5%	CC	Naghizadeh and Rice(1962)
84.5		1.58±0.08	ND	Dasannacharya and Rao(1965)
85.7	1.7	1.6 ±0.2	ND	Zandveld et al (1970)
85.2		1.73	ND	Skold as given by Van Loef (1972)
		B. Liquid krypton		
120.0	8.48	1.64±5%	CC	Naghizadeh and Rice (1962)
120.0	Saturation	$2.08^{+0.79}_{-0.61}$	NMR	Cowgill and Norberg (1976)

Note : CC - Capillary cell; ND - Neutron diffraction

NMR - Nuclear magnetic resonance

It can be seen that the experimental results for self-diffusion in liquids argon and krypton obtained so far are not in good agreement with each other. Consequently, there is a need for reliable and confirmatory data on diffusion in rare-gas liquids in general and argon and krypton in particular.

1.1 Purpose of the Present Study

The present work was undertaken with the objective of obtaining diffusion data in rare-gas liquids using the diaphragm cell method. It was performed in the same laboratory where this method was attempted earlier by Mills (1974). This attempt demonstrated the adaptability of the diaphragm cell method in the cryogenic temperature range. Instead of modifying the existing apparatus which had problems of temperature control and unnecessary sophistication, it was decided to construct an entirely new apparatus, however, retaining the experience on the earlier apparatus as a guide line.

The purpose of this thesis is:

a) to describe the design and development of an experimental facility consisting of a diaphragm cell with a provision for continuous monitoring of the diffusion of a radioactive tracer, and

b) to obtain tracer diffusion data for krypton in argon over a temperature range of 85 - 103 K and at pressures close to atmospheric.

1.2 Layout of the Thesis

The next chapter describes the construction of the apparatus. Mathematical treatment of equations from which the diffusion coefficient can be calculated for the case of continuous monitoring is given in Chapter 3. Chapter 4 contains the experimental procedures. Tracer diffusion data for krypton in argon over a temperature range of 85 - 103 K are reported in Chapter 5. Within the scope of the present study, the data are discussed in comparison to other experimental and computer simulation results in Chapter 6. Some suggestions for future work using the apparatus and conclusions derived from the study are given at the end of the thesis.

2. EXPERIMENTAL FACILITY

In this chapter the reasons for adapting the diaphragm cell method are enumerated. This is followed by a description of the design and construction of the diffusion cell, the stirring system, the temperature control system, the liquid argon filling method and a continuous monitoring system.

2.1 Choice of the Experimental Method

The diaphragm cell method was adapted for the following reasons:

i) the method has been found to be very accurate for studying tracer diffusion. The uncertainty in the measurement can be as low as 0.2% (Mills,1961),

ii) bulk flow of the liquid in the cell which is a source of high apparent diffusion coefficients (Mills,1974), can be reduced to an acceptable level, if not totally eliminated, through the use of a suitable temperature control system,

iii) it is possible to use larger cell volumes than in a capillary cell. Consequently, more tracer can be introduced into the cell which reduces the counting errors,

iv) because of reason iii) above, it is possible to incorporate a scintillation counting system right at the cell, eliminating the need to measure the concentrations of individual cell compartments at the end of an experiment, and

v) a single system made out of stainless steel can be used for atmospheric and high pressure experiments at cryogenic temperatures.

Although an earlier attempt to use the diaphragm cell technique for cryogenic liquids (Mills,1974) was less successful, the overall experience from that study could be gainfully used during the present development. The diaphragm cell method, however, suffers from certain disadvantages. For example, it is a relative method (needing calibration) compared to the capillary cell method which is an absolute one. The diaphragm cell method is very expensive for use with liquids such as krypton and xenon due to the comparatively large volumes needed.

The diaphragm cell in its modern form has been described by Stokes(1950). Details of the mathematical basis for the method and the normal experimental procedures have been described by Mills and Woolf (1968). A variation of the diaphragm cell to suit high pressure needs has been described by McCool (1971).

2.2 Experimental Apparatus

A cross-sectional view of the cryostat is shown in Figure 2.1. It consists of a copper vessel made in two parts - namely, the cylindrical part with the bottom dish and the top dome. All the rotating parts were supported from the bottom dish whereas the diaphragm cell and the connecting pipelines were anchored from the top dome. Copper was chosen as the material for the housing because of its high thermal conductivity and the ease with which it can be spun to shape from a 1.6 mm thick sheet. The physical dimensions of the vessel were chosen such that an annulus of 25 mm existed between it and the liquid nitrogen tank into which the vessel was suspended.

Threaded studs (36) were soldered on the flange of the copper vessel and free holes were provided on the flange of the

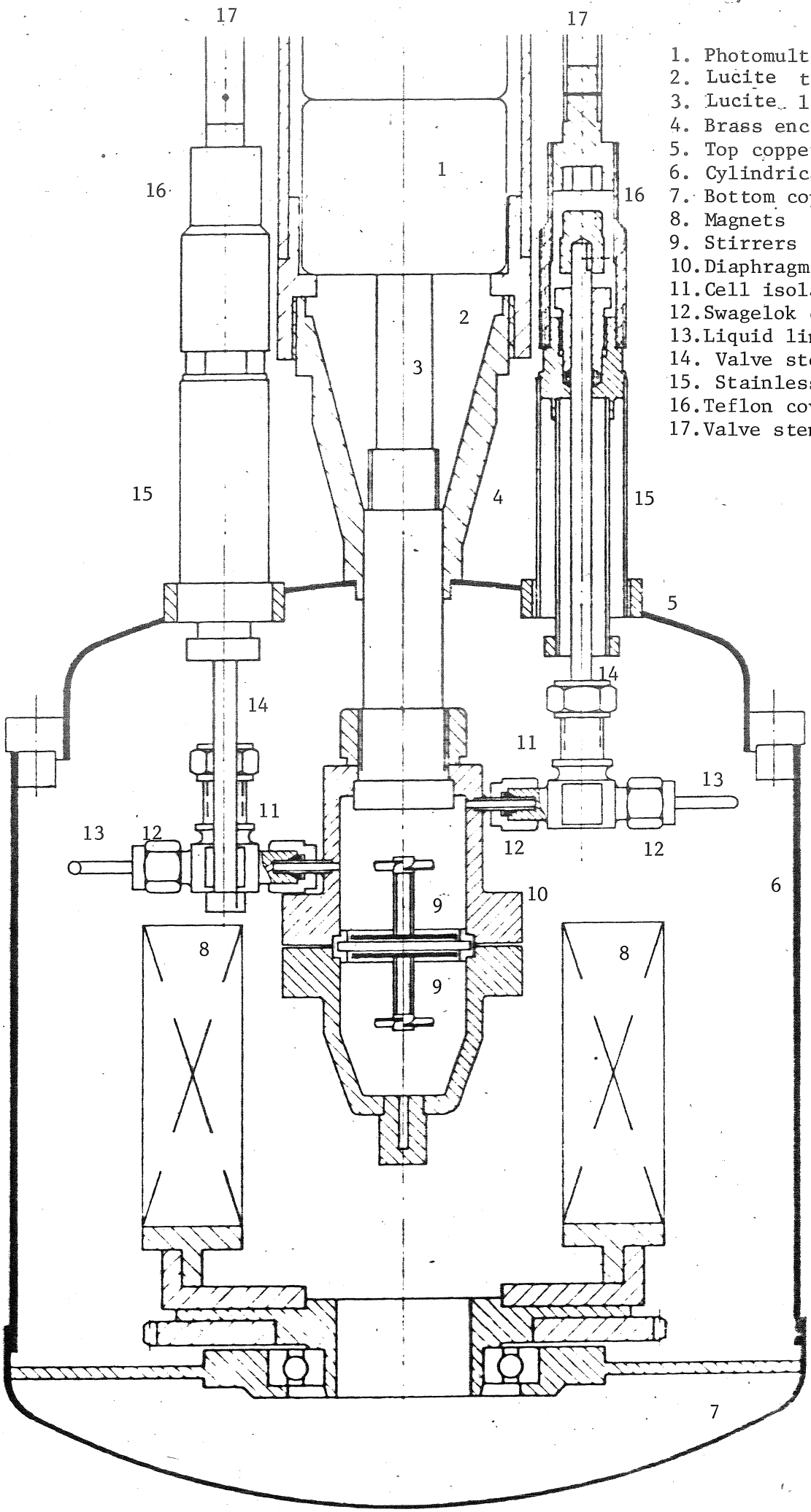

FIGURE 2.1 : A CROSS-SECTIONAL VIEW OF THE CRYOSTAT

top dome. The details of joining the two parts of the cryostat are shown in Figure 2.2. The entire assembly was suspended from a sandwich flange and immersed in a liquid nitrogen tank as shown in Figure 2.3. Photographic plate 1 shows the cryostat assembly prior to suspension into the LN2 tank and an overall view of the experimental facility.

2.2.1 Diffusion cell

The diffusion cell consisted of the following components: a) the top compartment with the liquid inlet and outlet lines, b) the bottom compartment with the liquid inlet line, c) the sinter assembly, d) the top and bottom stirrer assemblies and e) the cesium iodide crystal scintillator and the lucite light guide.

Stainless steel was chosen as the construction material in view of its high strength and fair ductility at cryogenic temperatures, its low coefficient of thermal contraction and a moderate thermal conductivity. The liquid volumes of the top and the bottom compartments were chosen to be about 25 cm^3 and 23 cm^3 respectively. Details of construction of the top and the bottom compartments are shown in Figures 2.4 and 2.5 respectively. The design criteria for the cell were the bursting forces due to internal pressure (taken as 500 bar max.), the sealing forces to be sustained by the flange and a need to provide a circumferentially uniform sealing on the flange. The liquid line diameters on the cell were chosen such that their contribution to the effective cell volume was small and yet the flow of liquid argon was not choked during filling operation.

The sintered stainless steel diaphragm had an effective pore volume of about 0.4 cm^3. Its construction is shown in Figure 2.6.

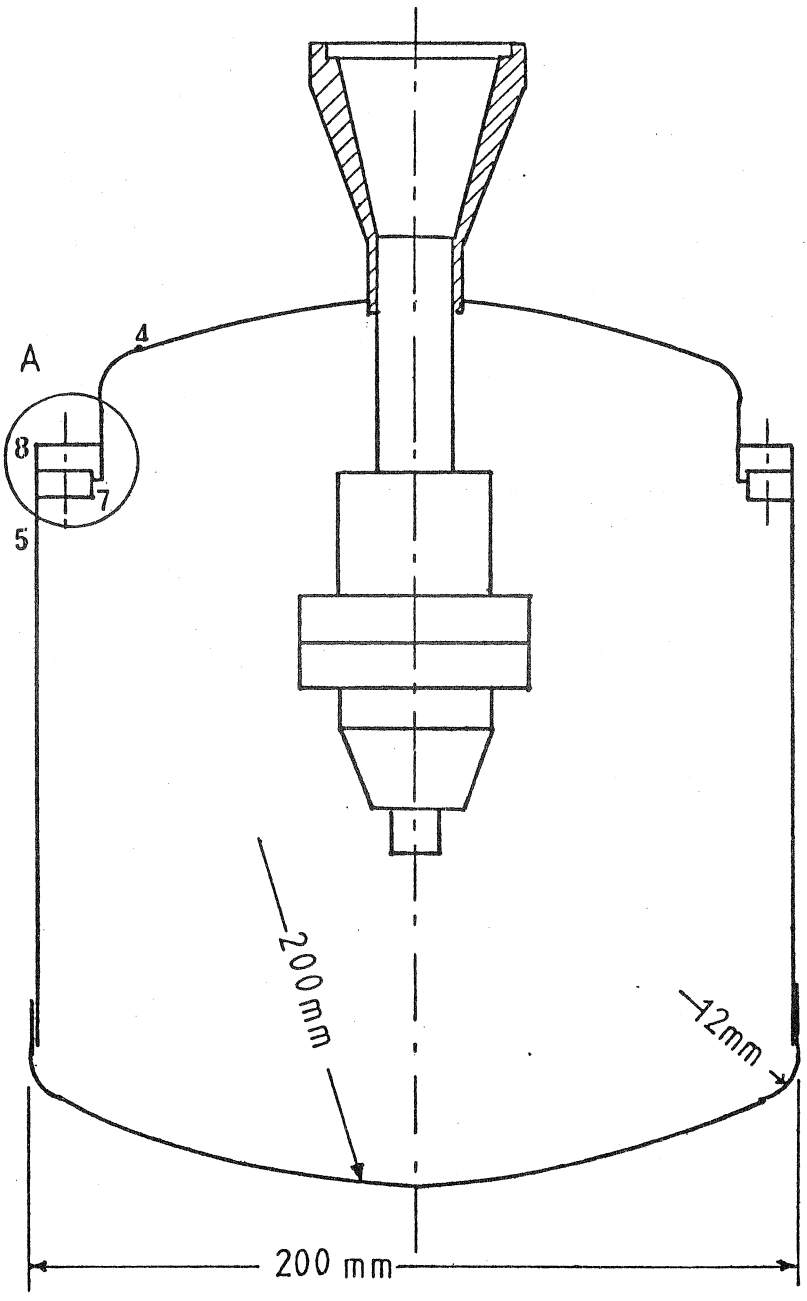

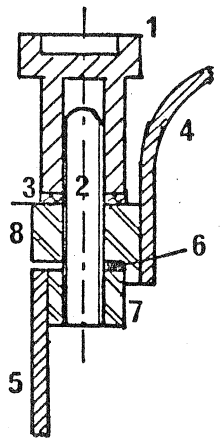

Details of A

1. Steel cap screw
2. Brass stud soldered to flange 7
3. Spring washer
4. Copper dome
5. Copper vessel
6. Indium o-ring
7. Flange on (5)
8. Flange on (4)

FIGURE 2.2 CRYOSTAT HOUSING

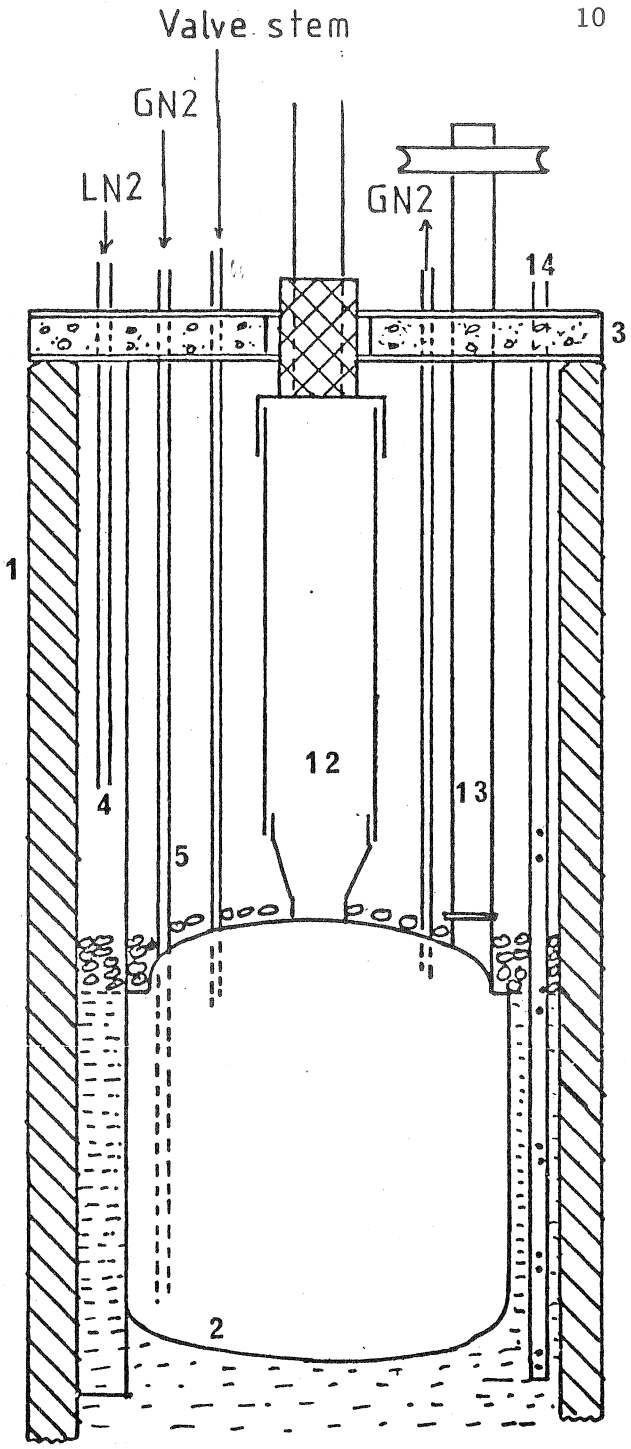

1. LN2 tank
2. Cryostat
3. Sandwich flange
4. LN2 line
5. GN2 line
6. L.Ar valve (bottom)
7. L.Ar valve (top)
8. L.Ar valve (top lower)
9. L.Ar line (bottom)
10. L.Ar line (top)
11. L.Ar line (top lower)
12. Photomultiplier
13. Drive shaft
14. Dipstick
15. Instrument lead port

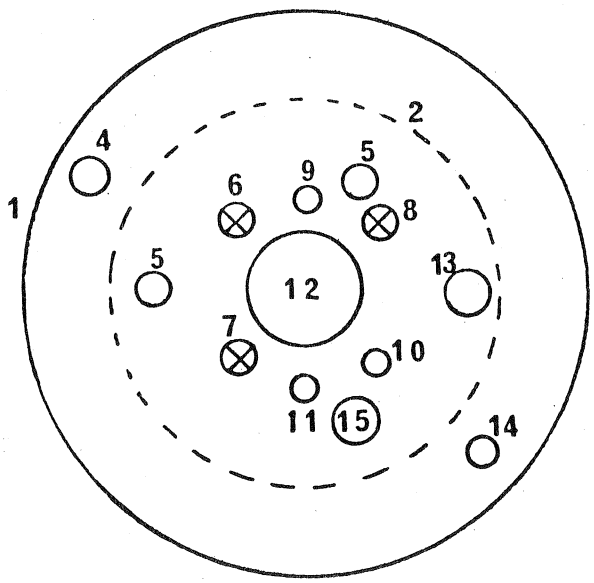

FIGURE 2.3 : CRYOSTAT SUSPENSION IN THE LN2 TANK

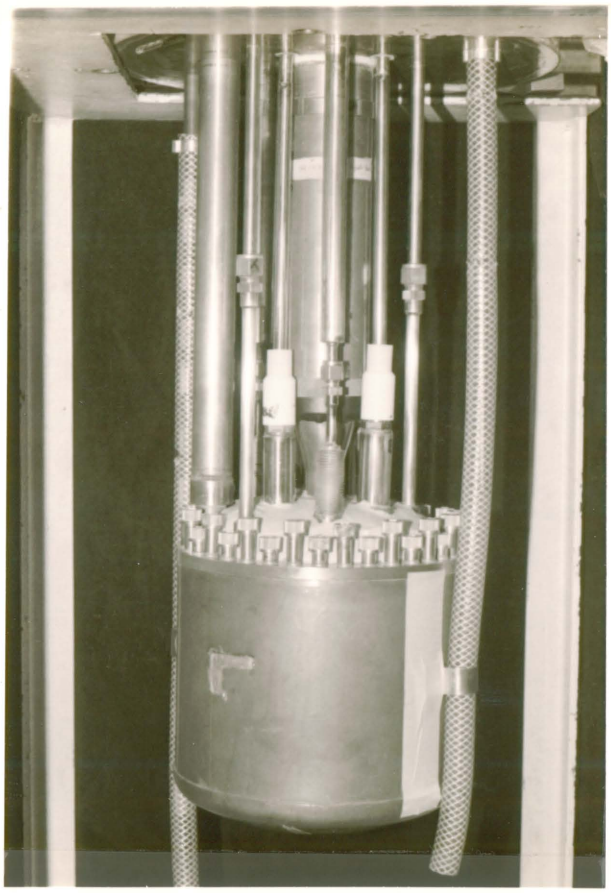

a. CRYOSTAT ASSEMBLY PRIOR TO IMMERSION INTO LN2 TANK

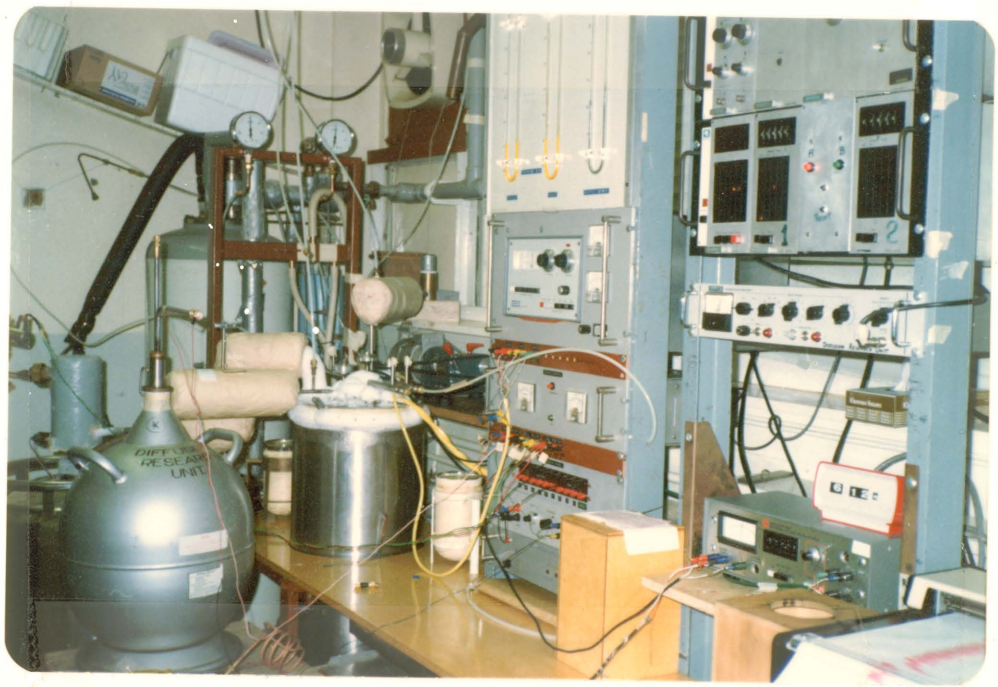

b) OVERALL VIEW OF THE EXPERIMENTAL FACILITY

Plate 1

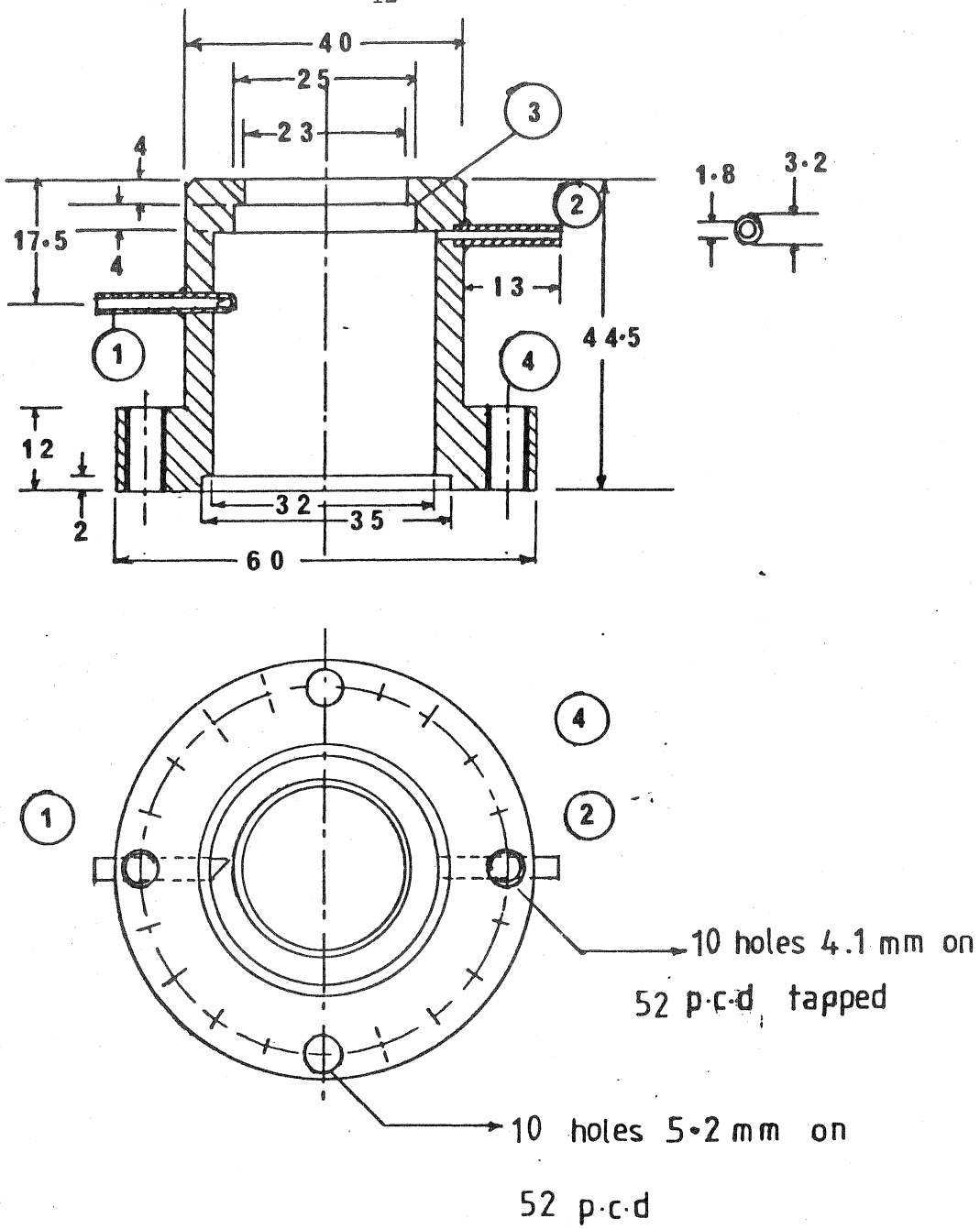

All dimensions are in mm

Material : 304 stainless steel

FIGURE 2.4 THE TOP COMPARTMENT

1. Liquid inlet line 2. Liquid outlet line
3. Opening for light guide assembly 4. Flange

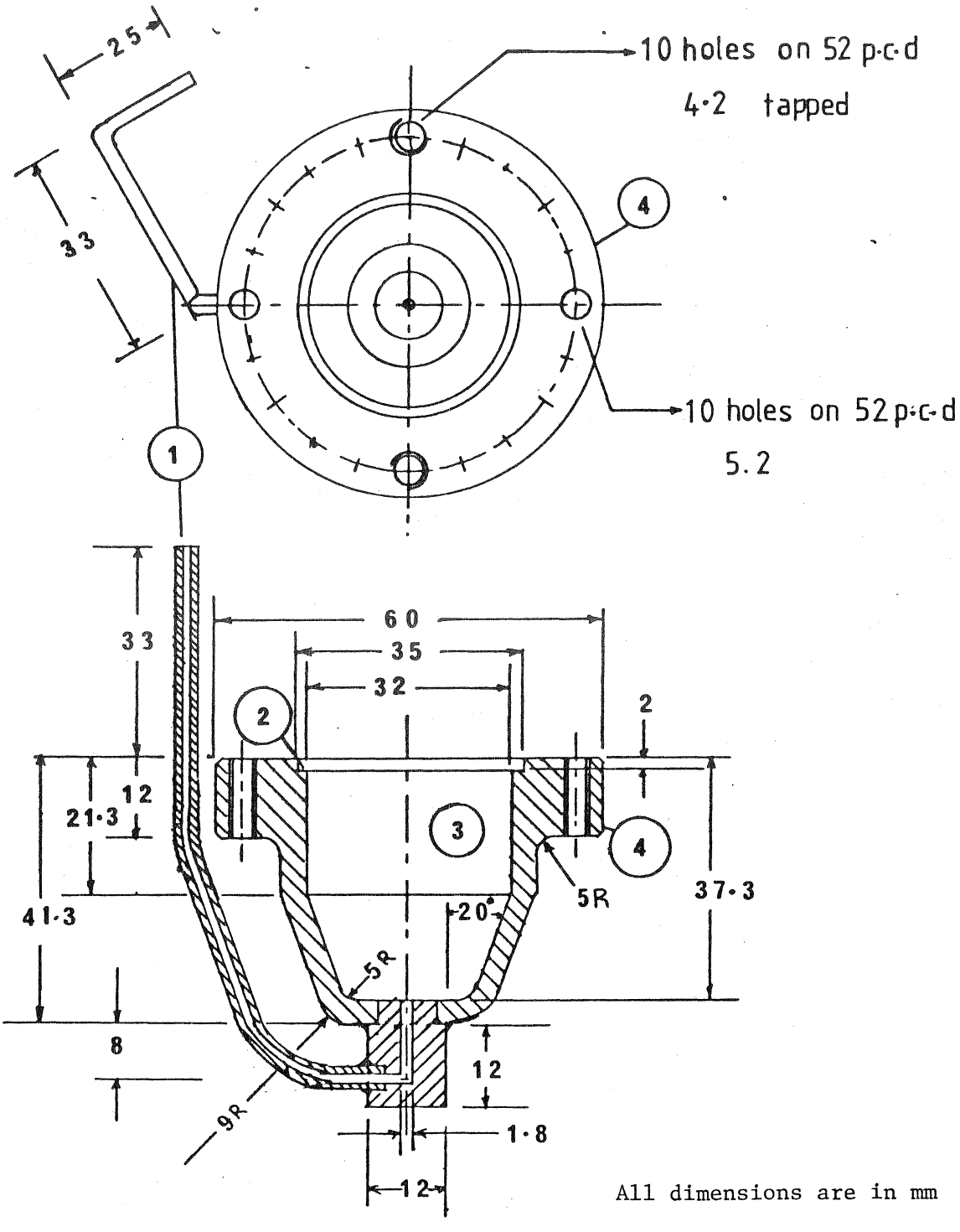

All dimensions are in mm

Material : 304 stainless steel

FIGURE 2·5 THE BOTTOM COMPARTMENT

1. Liquid line 2. Step for indium O-ring 3. Liquid volume 4. Flange

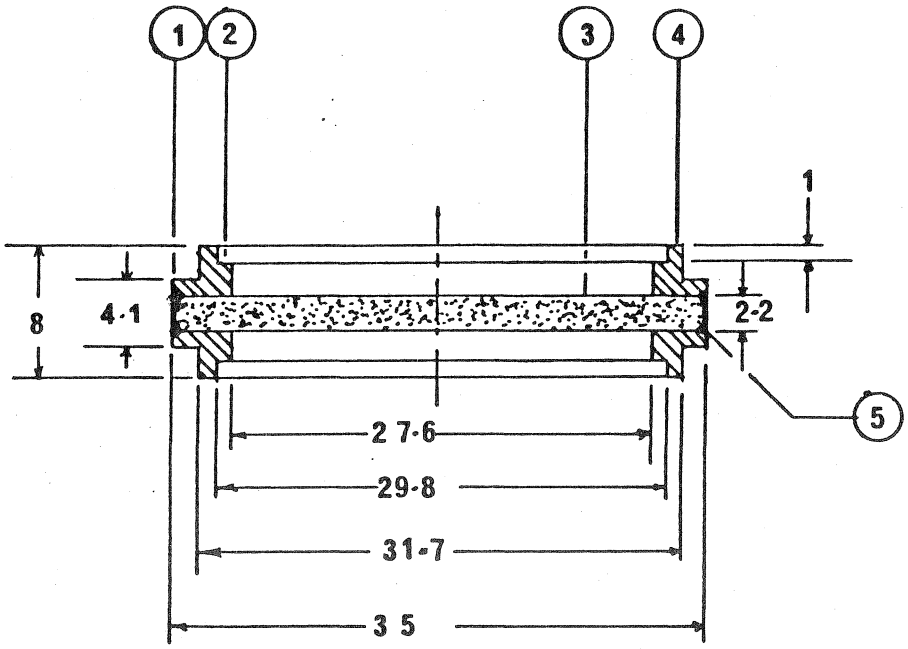

All dimensions are in mm

Material : 304 stainless steel except sinter which is 316L

FIGURE 2.6 SINTER ASSEMBLY

1. Outer step for indium O-ring
2. Inner step for stirrer body
3. Stainless steel sinter
4. Retaining ring
5. Peripheral weld to prevent radial diffusion

The mean pore size of the sinter was 5×10^{-6} m (No. 4) and the void volume was approximately 52%. To ensure that uniformity in concentration was maintained on either side of the sintered diaphragm in the cell compartments, a stirrer assembly was employed. The essential features of this assembly were the same as the ones used by McCool (1971) for high pressure diffusion studies on organic liquids. However, in the present case, the blades of the stirrers were hydrodynamically designed considering liquid argon as the working fluid. A stirring speed of 50 rpm was used which ensured substantial stirring without being too turbulent to disturb the liquid in the diaphragm. The stirrer system was made in three parts (Figure 2.7). No conventional lubricants were used between the rotor and the journal as they would freeze at liquid argon temperatures. Free running fits were provided between rotating and stationary components. When the entire assembly of the stirrers was placed in position, a gap of 0.3 to 0.5 mm existed between the face of the stirrer blade and the diaphragm. The rotor blade itself prevented the bottom stirrer from falling down. To prevent the top stirrer from falling on the sinter, a small paddle was screwed on the rotor shaft. The bottom stirrer was also provided with a similar paddle to maintain symmetry.

The scintillator crystal and the lucite light guide assembly were selected with the assumption that the experiments were to be conducted with Kr^{85} as the tracer. A machined and polished CsI crystal was mounted at the bottom end of the light guide. The assembly is shown in Figure 2.8. An indium O-ring was used to seal the joint between the lucite rod and stainless steel wall of the cell. The difference in the thermal contraction coefficients of lucite and stainless steel was found to enhance the sealing forces. The scintillator

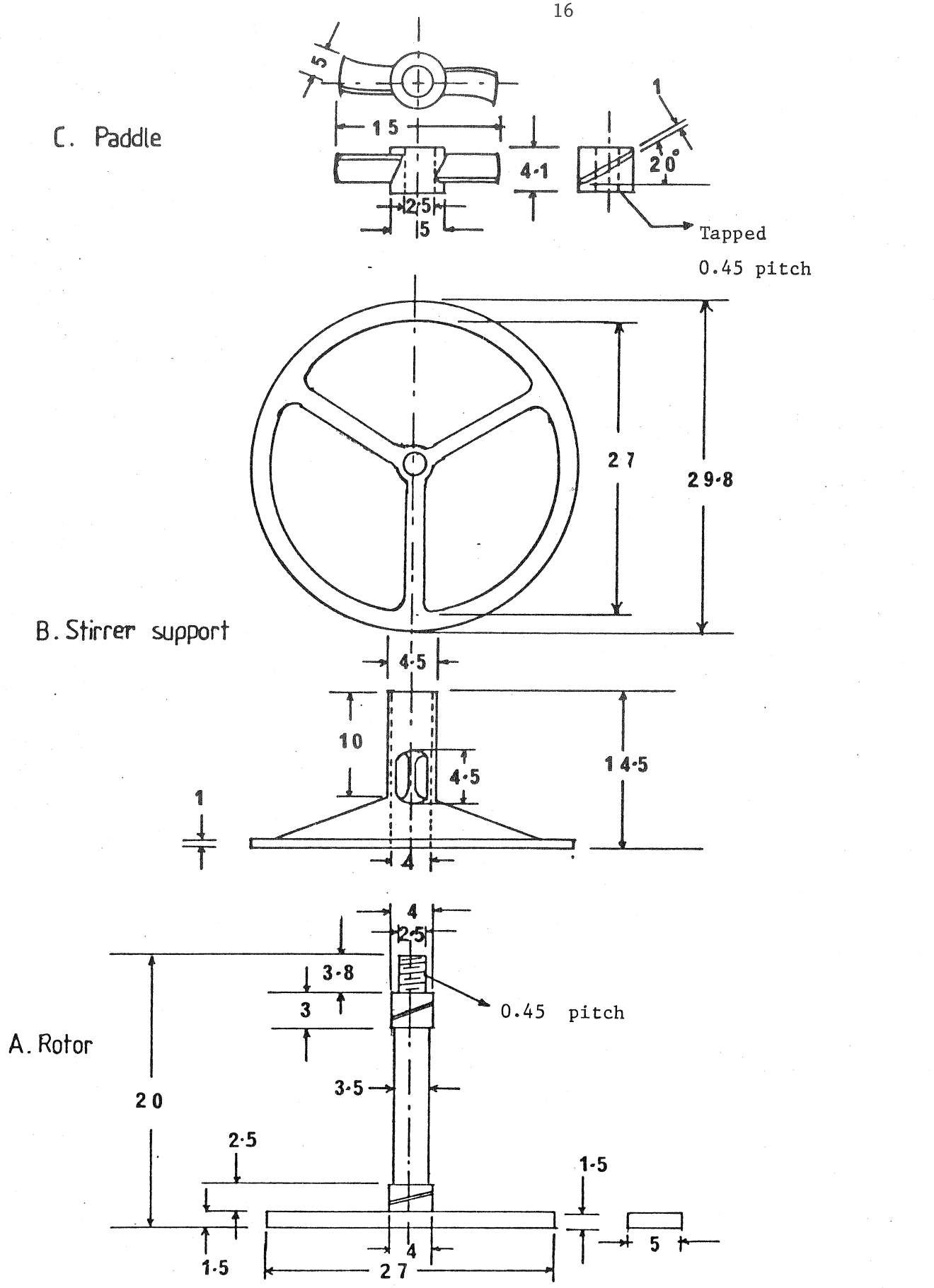

All dimensions are in mm

Material : Magnetic stainless steel

FIGURE 2.7 : STIRRER COMPONENTS

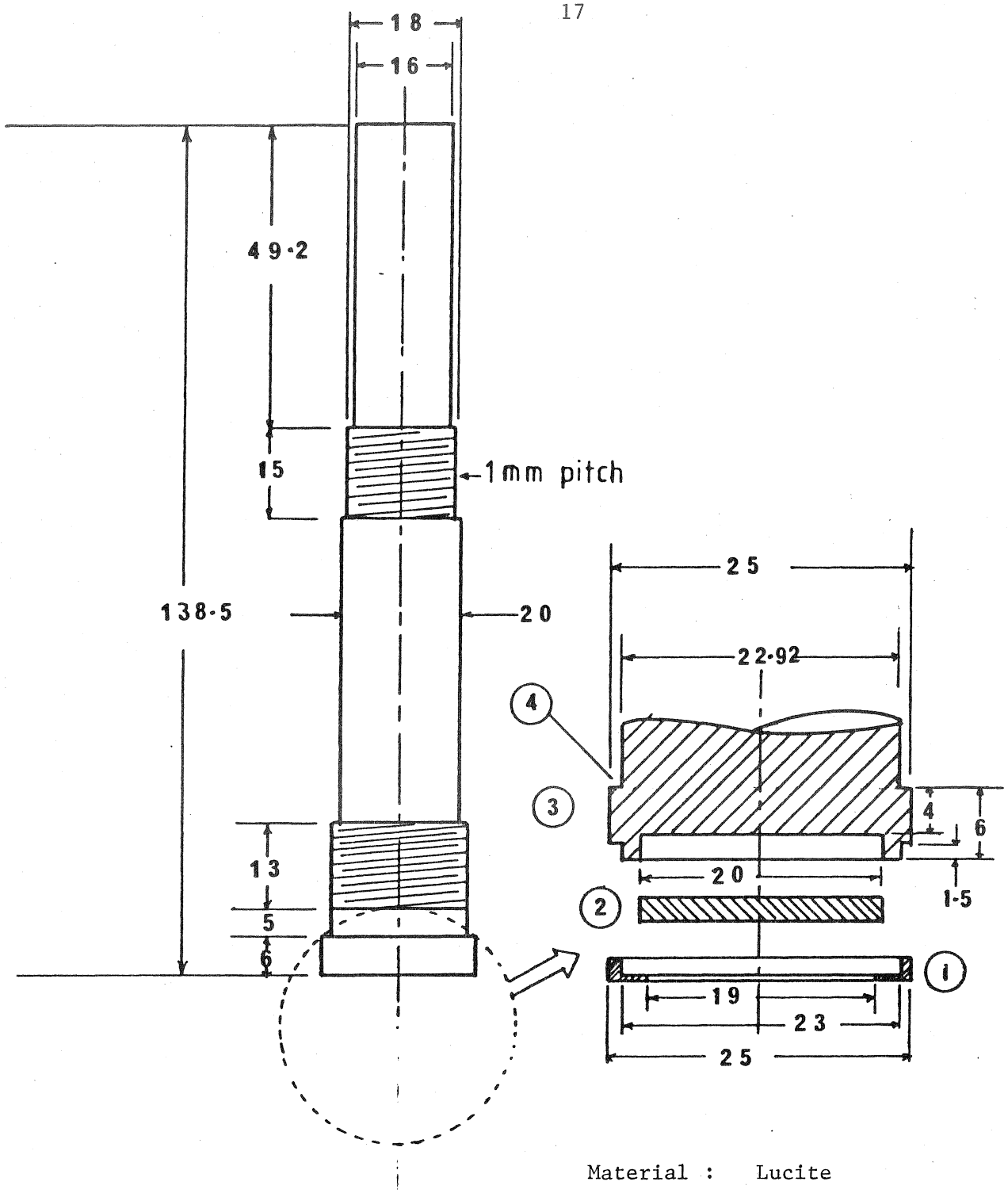

FIGURE 2.8 : LUCITE LIGHT GUIDE AND SCINTILLATOR ASSEMBLY

1. Retaining ring
2. Cesium Iodide crystal
3. Light guide
4. Step for O-ring

projected into the liquid volume of the top compartment to ensure a positive contact between it and liquid argon.

The cell was assembled using 5 mm cap screws. For operation up to a pressure of 100 bar, 10 cap screws were found to be sufficient. Each cap screw was tightened to a torque of 2.5 Nm. Indium O-rings were used at appropriate locations to provide effective seals for liquid in the cell.

The liquid lines on the top and the bottom compartments were connected to Whitey Model OS-OVS 2 (1/8" nominal) stainless steel valves through Swagelok connections. The commercial form of the valve was modified to suit the requirements of operation at cryogenic temperatures. After assembly, the cell was leak tested using gaseous argon up to a pressure of 20 bar at room temperature. Photographic plate 2 shows the cell and its components prior to assembly. The calibration procedure for the cell will be detailed in Chapter 4.

2.2.2 The stirrer drive system

The stirrer drive system played two important roles in the present design. Firstly, through a magnetic coupling it rotated the stirrer rotors inside the cell and secondly, it provided the necessary turbulence in the gas volume of the cryostat so as to enable maintainance of a uniform temperature zone around the cell. The stirrer drive system is depicted in Figure 2.9. The vertical positioning of the magnets was determined after obtaining the flux plots for a given pair of magnets. The radial position of the magnets could be adjusted by locating the yoke on a sliding passage. The radial positioning was determined considering the concentricity of the circles of rotation of the two magnets and the need to avoid dynamic imbalance.

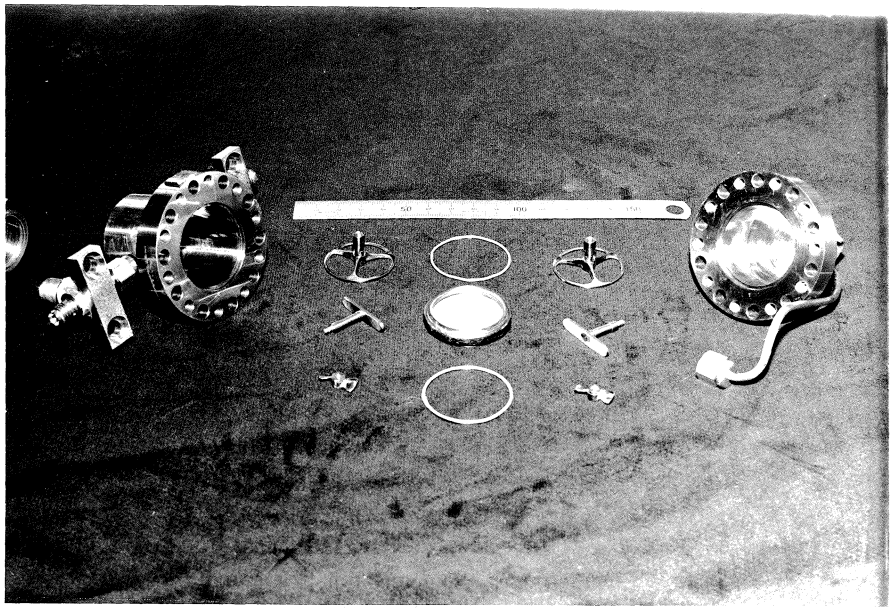

a) THE DIAPHRAGM CELL AND ITS COMPONENTS

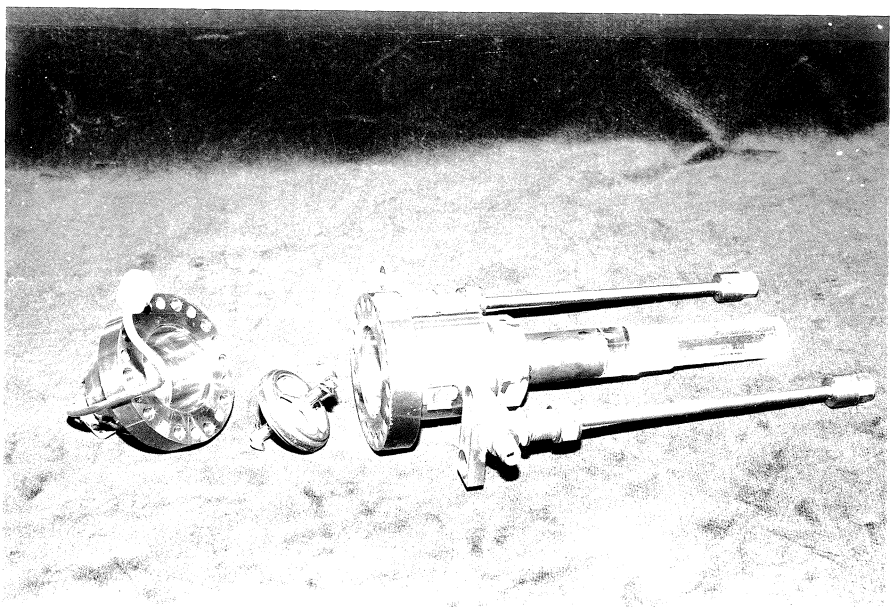

b) CELL PRIOR TO ASSEMBLY

PLATE 2

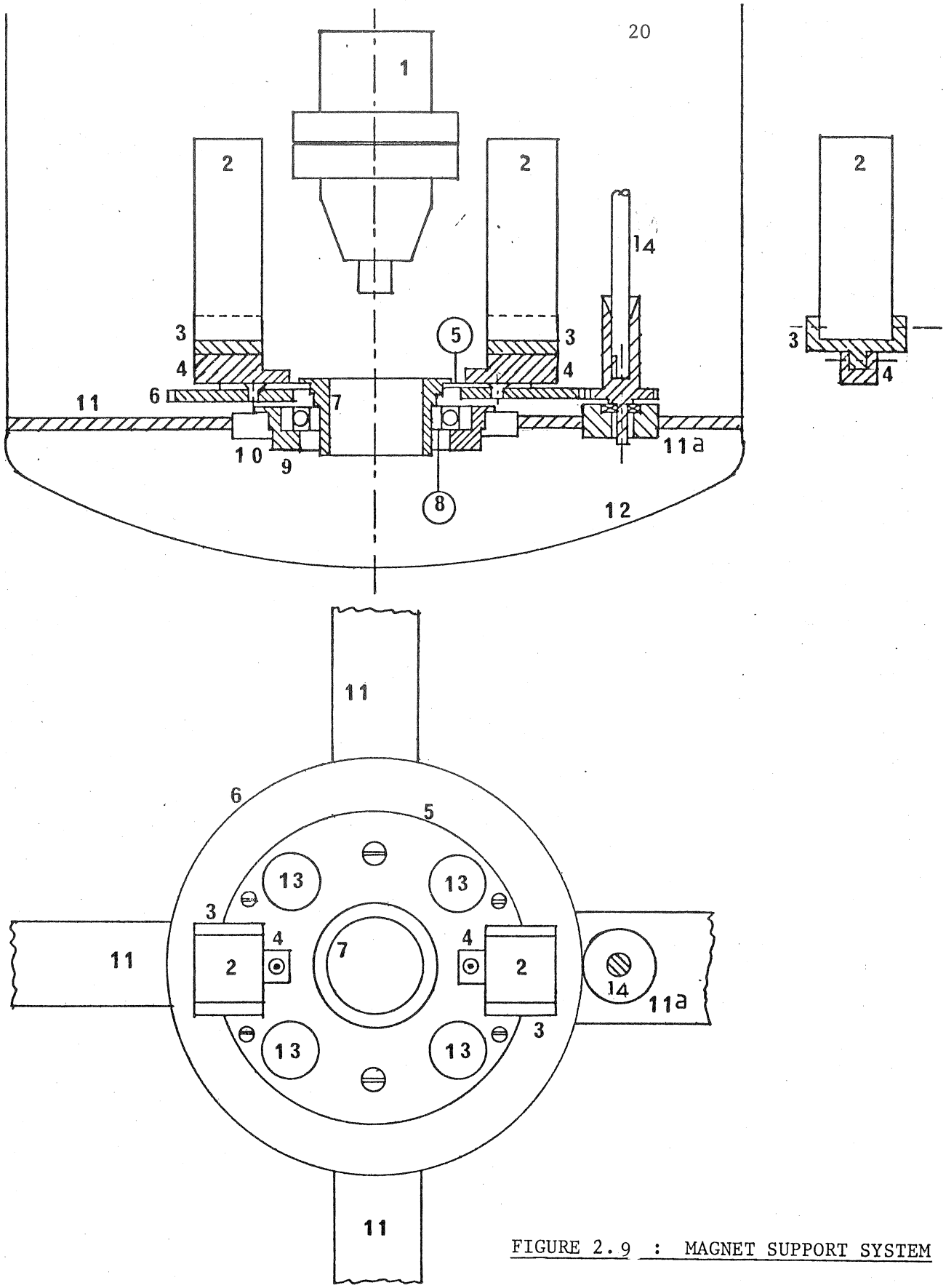

FIGURE 2.9 : MAGNET SUPPORT SYSTEM

1. Cell 2. Magnets 3. Yoke 4.Yoke slide guide 5. Brass plate

6. Gear wheel 7. Stainless steel hub 8. Ball bearing

9. Stainless steel journal 10. Brass support 11. Brass strut

11a. Pinion support 12. Copper vessel 13. Holes to reduce weight

14. Main drive shaft

The magnet support system was held by the inner race of a ball bearing. The ball bearing was positioned on a frame which was soldered to the bottom dish of the cryostat. Since the conventional lubricants are solid at cryogenic temperatures the steel balls of this bearing were replaced by teflon balls.

The main drive shaft of the system is shown in Figure 2.10. The shaft derived its motion from an electric motor through a reduction gear box and a belt driven pulley. The overall length of the drive shaft was 610 mm. Consequently, it had to be supported at a few other locations as shown in the figure. To prevent the ambient air leaking into the cryostat, suitable sealing methods were employed . Photographic plates 3 and 4 show the details of the stirrer system.

2.2.3 The temperature control system

A precise control of temperature of the diffusion cell over prolonged periods of time was a notable feature of the present development. The technique employed was to use a continuous gas flow to control the heat leak to the cell (Godwin,1960 and Blancett and Canfield, 1966).

The temperature control system can be divided into the following subsystems: a) temperature sensing elements, b) the heating system and c) the cooling system.

A. Temperature sensing elements

Platinum resistance thermometers were chosen as the sensors due to their high stability and a fairly linear relationship between resistance and temperature in the range of

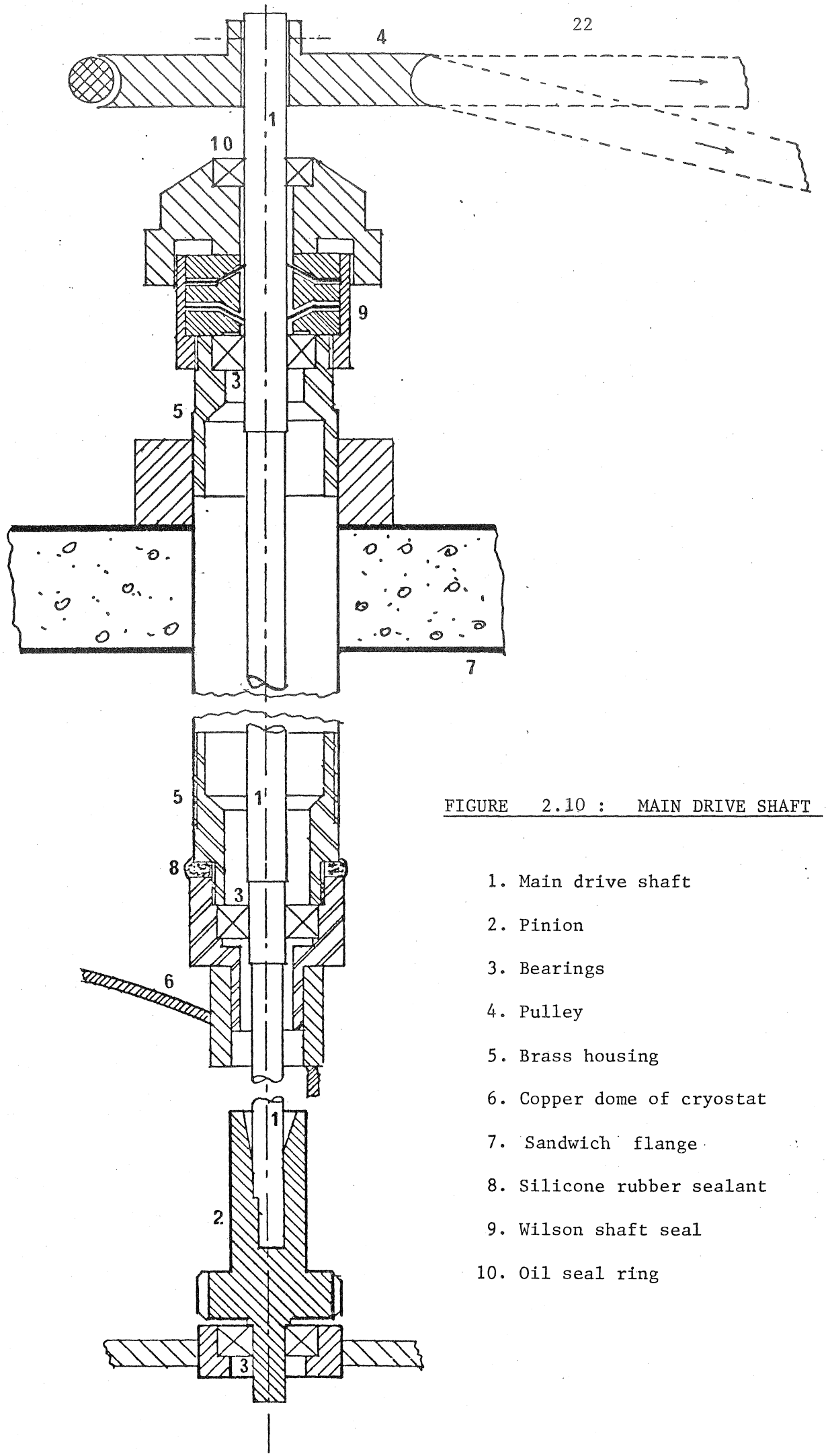

FIGURE 2.10 : MAIN DRIVE SHAFT

1. Main drive shaft
2. Pinion
3. Bearings
4. Pulley
5. Brass housing
6. Copper dome of cryostat
7. Sandwich flange
8. Silicone rubber sealant
9. Wilson shaft seal
10. Oil seal ring

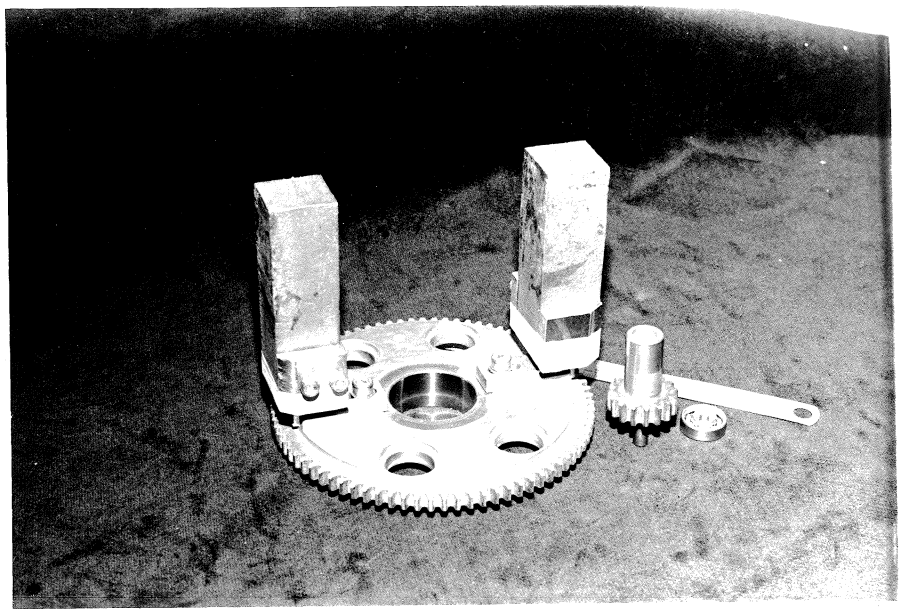

A) MAGNETS, GEAR AND PINION OF THE STIRRER SYSTEM

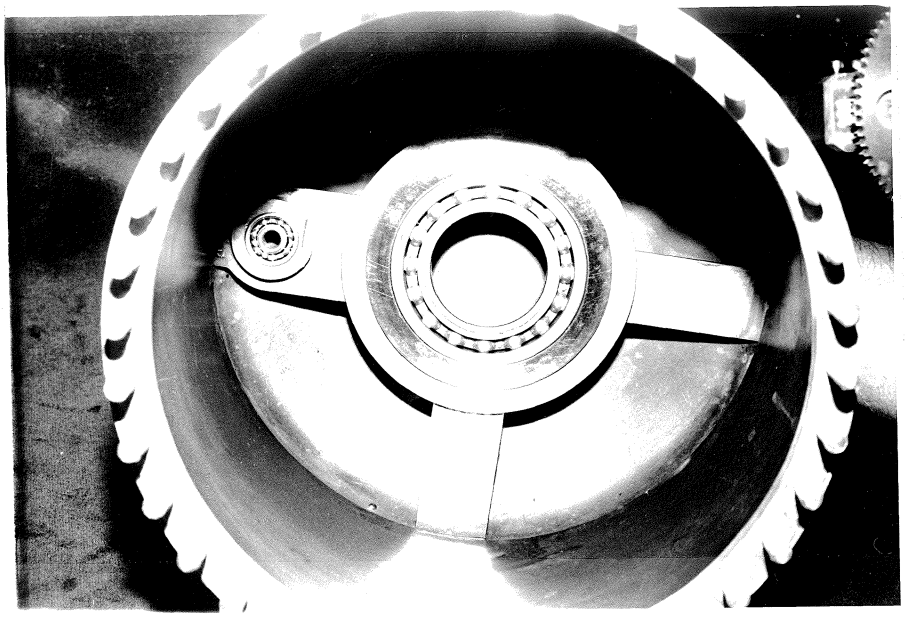

B) STRUTS AND BEARING OF THE STIRRER SUPPORT SYSTEM IN THE COPPER VESSEL OF THE CRYOSTAT

PLATE 3

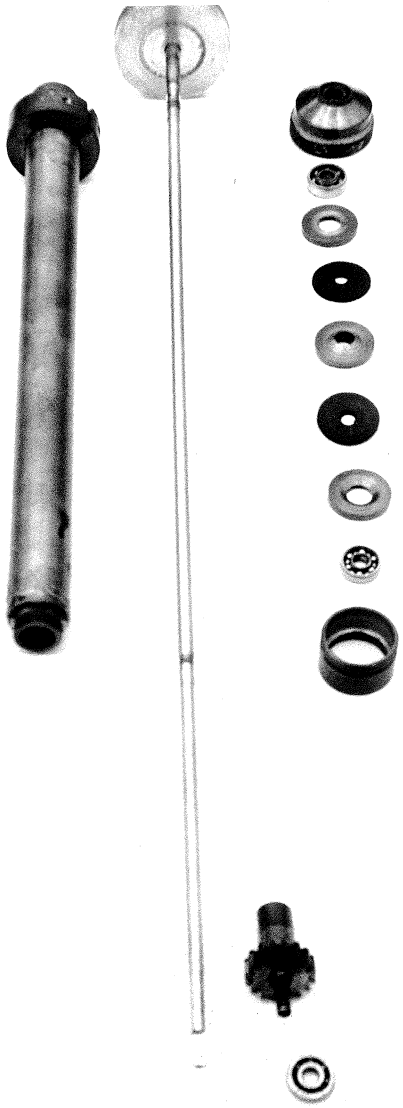

THE MAIN DRIVE SHAFT AND ITS COMPONENTS

PLATE 4

85 - 150 K. The aim was to obtain a stability of ± 0.03 K. Using a commercially available temperature measuring resistance bridge it was possible to realise this precision.

One platinum sensor was mounted on the outer surface of the top compartment and another on the conical surface of the bottom compartment. To reduce the effect of magneto-resistance due to the rotating magnets the sensors were shielded using mu-metal strips.

Type T (copper-constantan) thermocouples were used to obtain the information on temperatures at various radial and axial locations on the cell and in the cryostat volume. They were placed at the following locations: i) outer surface of the top compartment (one near the light guide and one near the flange), ii) outer surface of the bottom compartment (one on the cylindrical part and one on the conical part), iii) one each on the flanges of the cell, iv) one on the cell isolation valve located in the liquid exit line of the top compartment, v) inner surface of the top dome where the light guide passes through, vi) gas volume of the cryostat adjacent to the light guide and vii) outer surface of the brass housing of the photo-multiplier tube (one at the top end and one at the bottom end). They provided a useful check on the temperature distribution in the cryostat. These data were used extensively to locate the sources of thermal instability in case of a faulty operation.

B. The heating system

A schematic diagram of the heating system is shown in Figure 2.11. Liquid nitrogen was used as a coolant since the diffusion experiments were intended to be performed with liquid argon. The inherent tendency of the cell was to cool. The temperature control

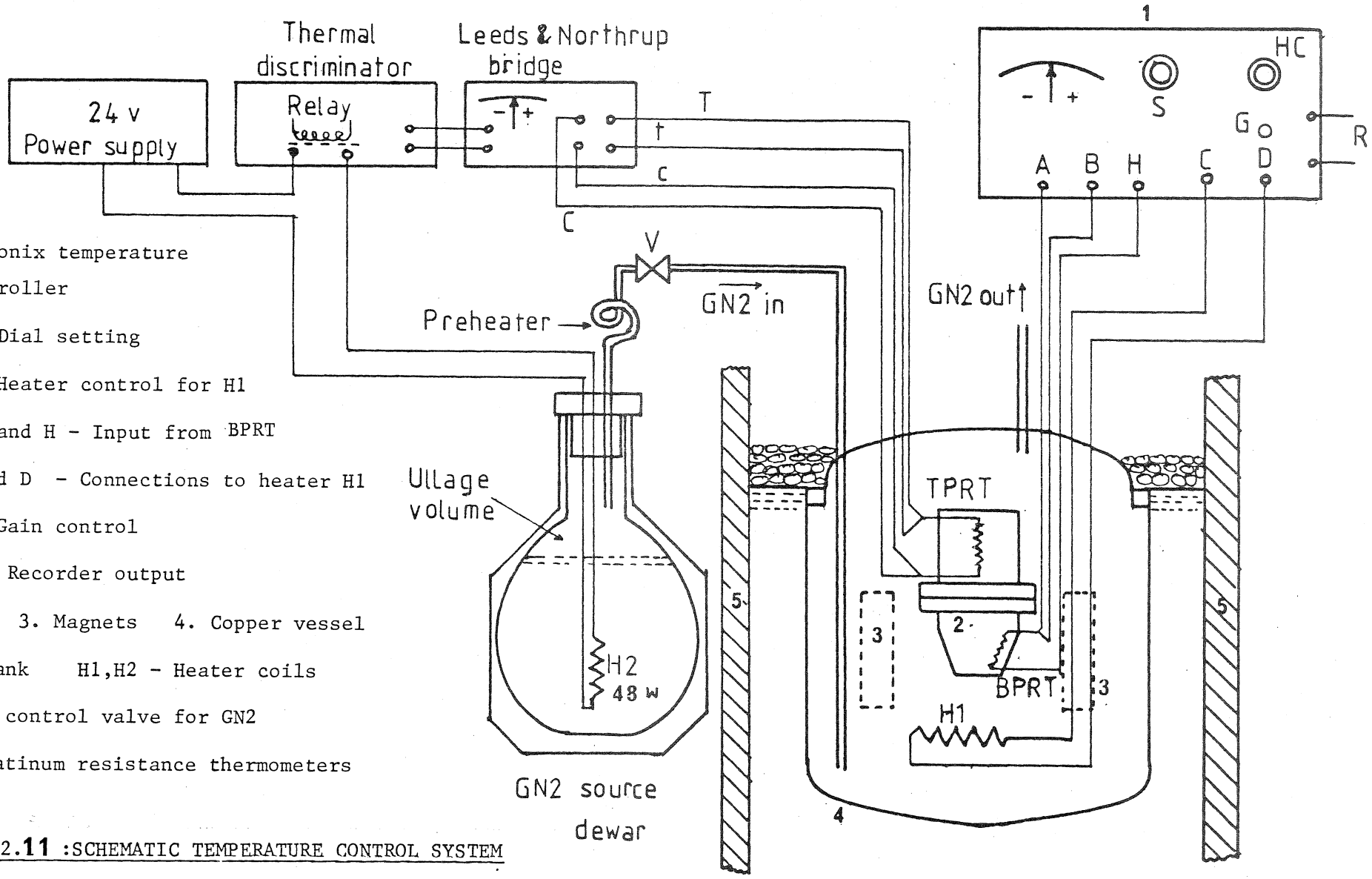

1. Artronix temperature controller

   S - Dial setting

   HC- Heater control for H1

   A,B and H - Input from BPRT

   C and D - Connections to heater H1

   G - Gain control

   R - Recorder output

2. Cell 3. Magnets 4. Copper vessel

5. LN2 tank H1,H2 - Heater coils

V - Flow control valve for GN2

PRT - Platinum resistance thermometers

FIGURE 2.**11** :SCHEMATIC TEMPERATURE CONTROL SYSTEM

system was designed to bring the temperature of the cell to a set point and to hold it at that level during an experiment within the limits specified earlier.

Inside the cryostat a base heater (H1) was suspended from the liquid line on the bottom compartment. The construction of the heater is shown in Figure 2.12. The heater suspension can be seen on Photographic plate 5. The heater was made of nichrome wire to give an overall resistance of about 54 ohms. At the maximum power output of the Artronix temperature controller this base heater was capable of dissipating up to 50 W. However, under normal operating conditions the heat dissipated seldom exceeds 6 W. The additional heating capacity provided for a rapid raise in temperature, if necessary. The amount of heat dissipated in the heater, H1, was controlled by the Artronix temperature controller (Model 5301). The sensing element for this instrument is the platinum resistance thermometer (BPRT) on the bottom compartment.

The gas flow through the cryostat was manipulated by on/off control of heater H2 in the gaseous nitrogen dewar. This heater had a capacity of 48 W. The switching sequence of the heater was controlled by a thermal discriminator. This instrument had a provision for adjusting the threshold and hysteresis which control the duration for which the heater circuit relay was kept closed. The relay would close when the input d.c signal to this instrument was above the threshold. It would remain so until the input signal had receded to the level of the threshold, if the hysteresis is zero. For maximum hysteresis, the relay would stay closed until the input signal was equal to zero. The operation of the controls is explained in Figure 2.13.

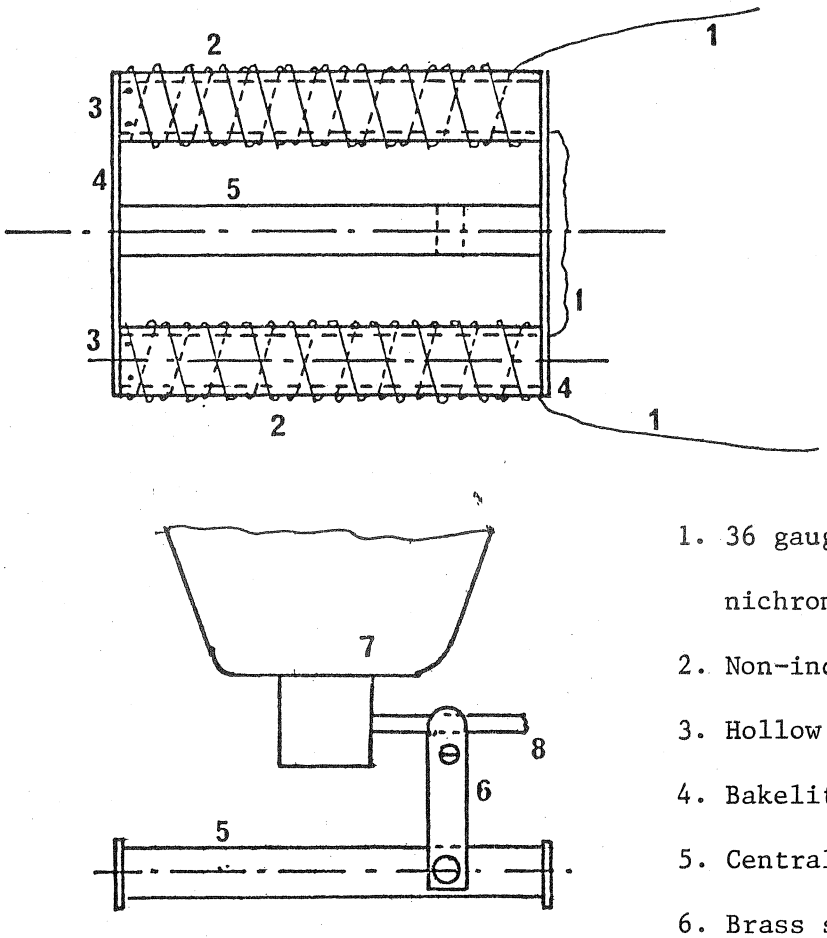

1. 36 gauge (0.226 mm) nichrome wire
2. Non-inductive winding
3. Hollow bakelite mandrel
4. Bakelite strips
5. Central suspension mandrel
6. Brass suspension arm
7. Cell bottom compartment
8. Liquid line

FIGURE 2. 12 : BASE HEATER AND ITS MOUNTING

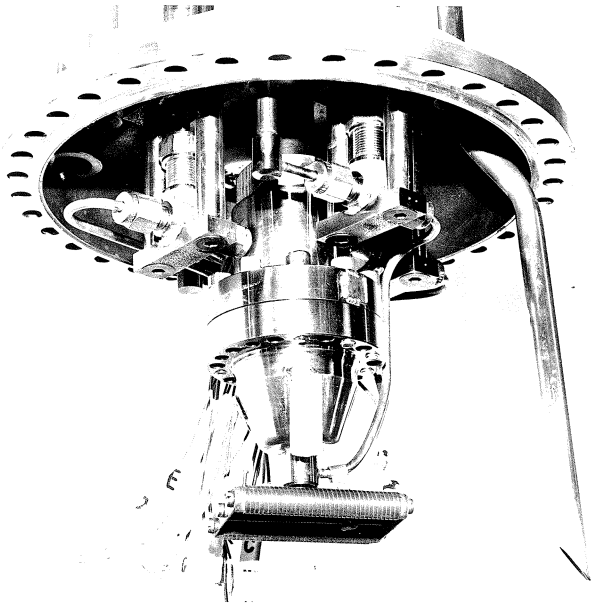

SUSPENSION OF CELL FROM THE TOP COPPER DOME OF THE CRYOSTAT

PLATE **5**

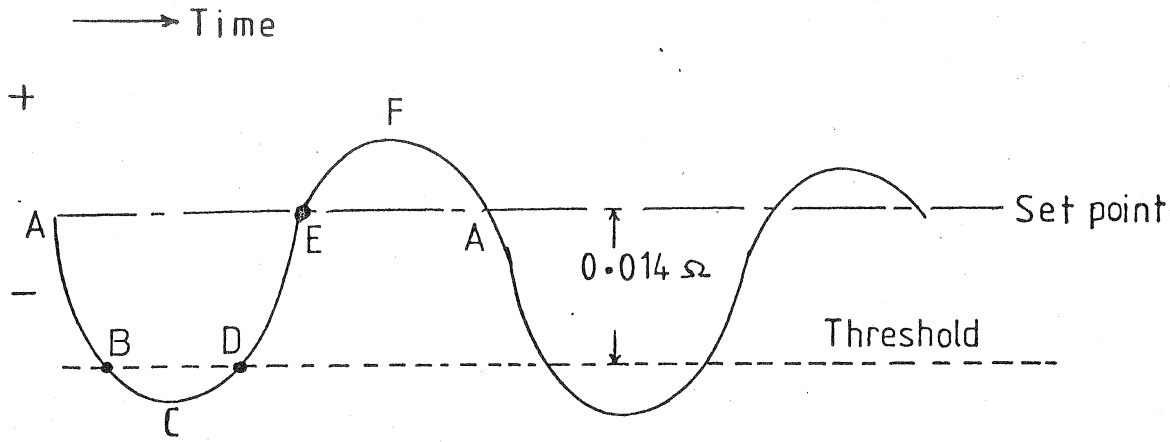

B - Heater H2 turned on D - Heater H2 turned off for no hysteresis

E - Heater H2 turned off for maximum hysteresis

ABCDEFA - Typical cycle of temperature

BCD - thermal time lag during initiation of gas flow

EFA - thermal time lag during stopping of gas flow

a) Temperature cycle details

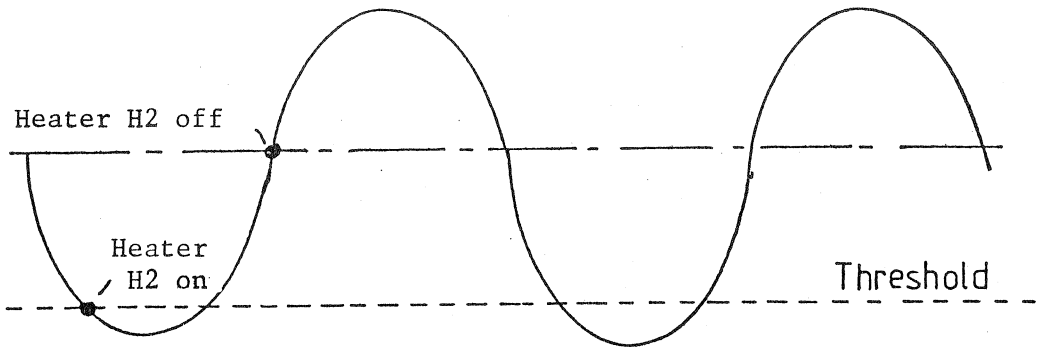

b) Temperature cycle for maximum hysteresis(large cycle time and fluctuations)

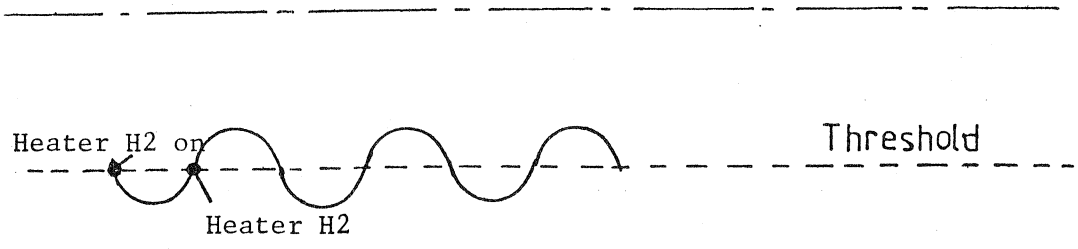

c) Temperature cycle for zero hysteresis(small cycle time and fluctuations)

FIGURE 2. 13 : THERMAL CYCLING OF THE CELL

The thermal discriminator derived its input from a Leeds and Northrup (L & N) bridge. This bridge had the platinum resistance thermometer on the top compartment (TPRT) as a sensor. When the temperature of the top compartment went below 0.03 K from the set point, the relay in the heater (H2) circuit would close. This resulted in evaporation of liquid nitrogen in the dewar. A preheater was located in the GN2 line to raise the temperature of the gas to that of the ambient condition. A valve was located in the line to control the volumetric flow rate of the gas. Due to a flow of warm nitrogen gas through the cryostat, the cell temperature would increase. When it had reached the set point within 0.03 K, the heater circuit would open resulting in a decrease in gas generation in the dewar. However, the flow of GN2 would continue due to pressure difference between the vapour space of the dewar and the cryostat. The rotating magnets in the cryostat would provide enough turbulence around the cell so that a uniform temperature was attained over the entire cell.

C. The cooling system

The schematic arrangement of the LN2 cooling system for the cryostat is shown in Figure 2.14. The level of liquid nitrogen was maintained around the flange of the copper vessel. A constant level was ensured by the use of a thermistor level sensor and a liquid nitrogen level controller. The source of LN2 was a 75 litre dewar. It was necessary to avoid any ripples on the free surface of liquid nitrogen when the liquid was being transferred into the tank. This was achieved by using a phase separator arrangement and by using polystyrene balls on the LN2 surface. The latter arrangement was also found to minimise the evaporation loss considerably. The LN2 filling cycle is shown in Figure 2.15.

1. Cell
2. Copper vessel
3. GN2 lines
4. Liquid nitrogen line
5. Dipstick
6. Insulated transfer line
7. 24 v, 10 W solenoid valve
8. LN2 tank
9. Sandwich flange
10. Polythene hose
11. Polystyrene board

TP - Thermistor pair

E - Earth/common

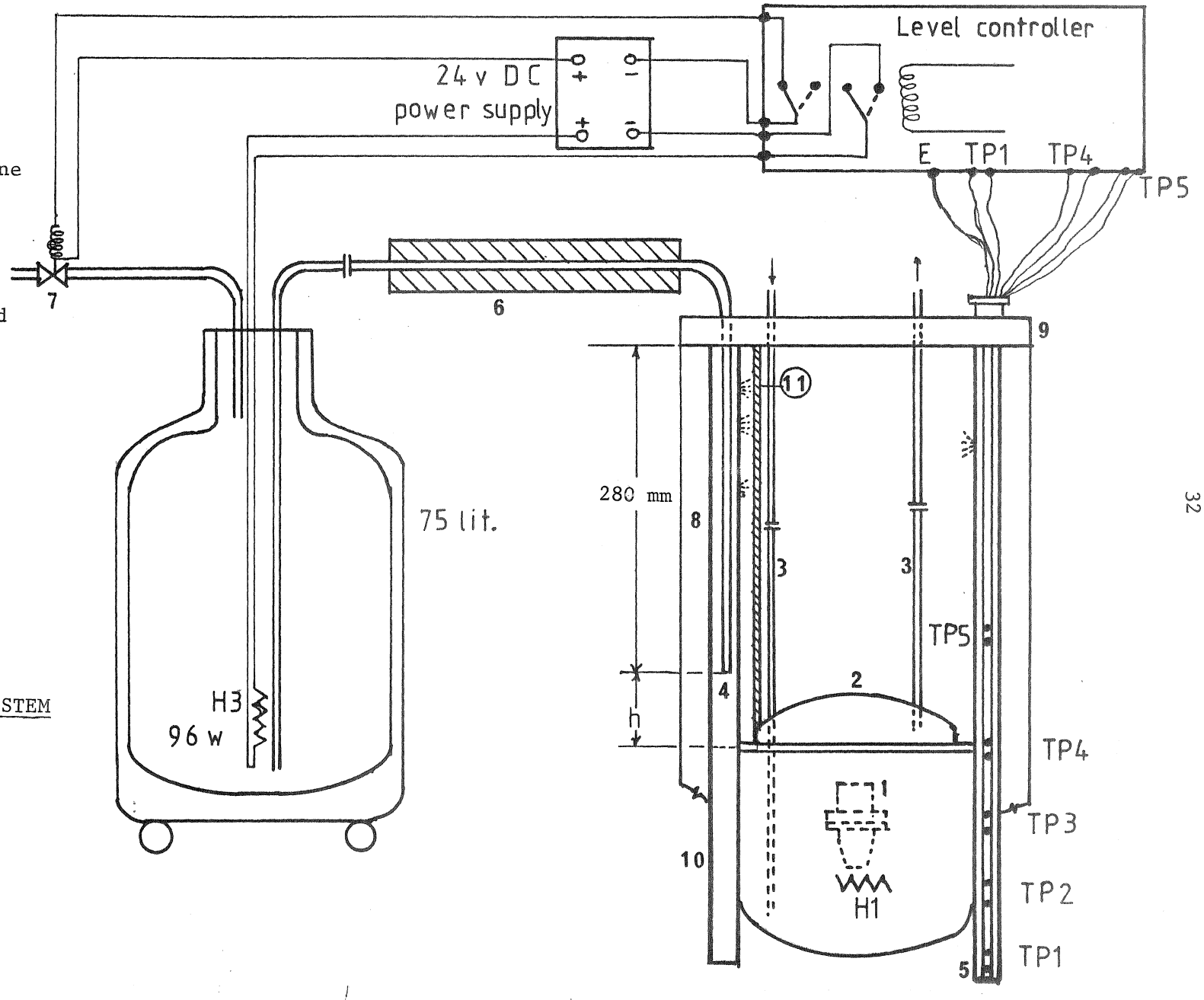

FIGURE 2. 14 :

SCHEMATIC LN2 FILLING SYSTEM

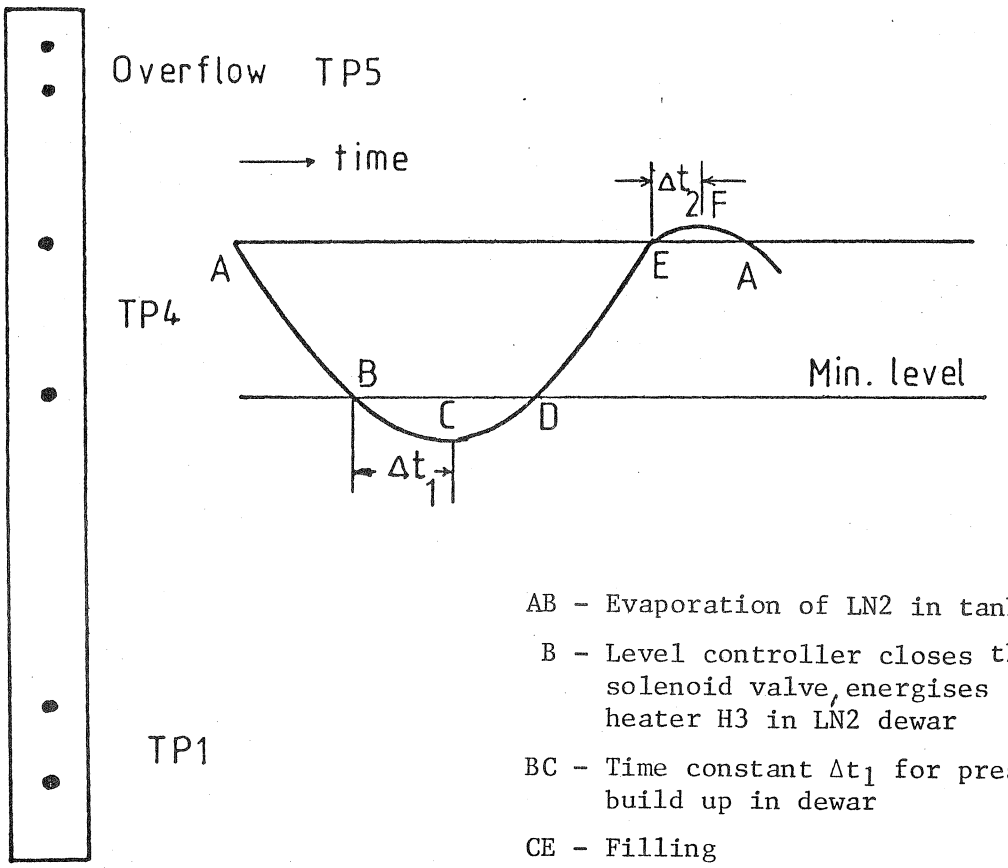

AB - Evaporation of LN2 in tank

B - Level controller closes the solenoid valve, energises heater H3 in LN2 dewar

BC - Time constant Δt_1 for pressure build up in dewar

CE - Filling

E - Solenoid valve is opened and power to heater H3 is cut off

EF - Δt_2, time constant to release dewar pressure

FIGURE 2.15: LN2 FILLING CYCLE

2.2.4 Liquid argon filling system

The present development differs from the previous experimental methods in the sense that here liquid argon was condensed outside the cell and then transferred into it using the pressurised transfer method.

The schematic liquid argon filling system is shown in Figure 2.16. The bottom and the top compartments were connected to liquid lines through 1/8" nominal pipes. The liquid lines were introduced into the cryostat through a brass bellows arrangement on the copper dome as shown in Figure 2.17. The brass bellows was to accommodate thermal contraction during cool-down of the cryostat. Swagelok connections were used in the pipelines for the ease of assembly. A part of the liquid argon transfer line outside the copper vessel was vacuum insulated. The jacket vacuum was maintained below 0.06 torr by using a rotary vacuum pump. Relatively shorter sections of the transfer line were left uninsulated.

Although Figure 2.16 shows the arrangement for a top loaded run, a bottom loaded run could be made possible through appropriate changes.

Stainless steel flasks, of 470 cm^3 capacity each, were used to collect condensed argon. The condensation was achieved by allowing gaseous argon to flow through a copper coil immersed in an LN2 bath. The actual filling operations will be described in Chapter 4.

A. Method of introducing radioactive tracer into the cell

The radioactive tracer (Kr^{85}) was injected into a stream of liquid argon flowing from the flask to the top compartment

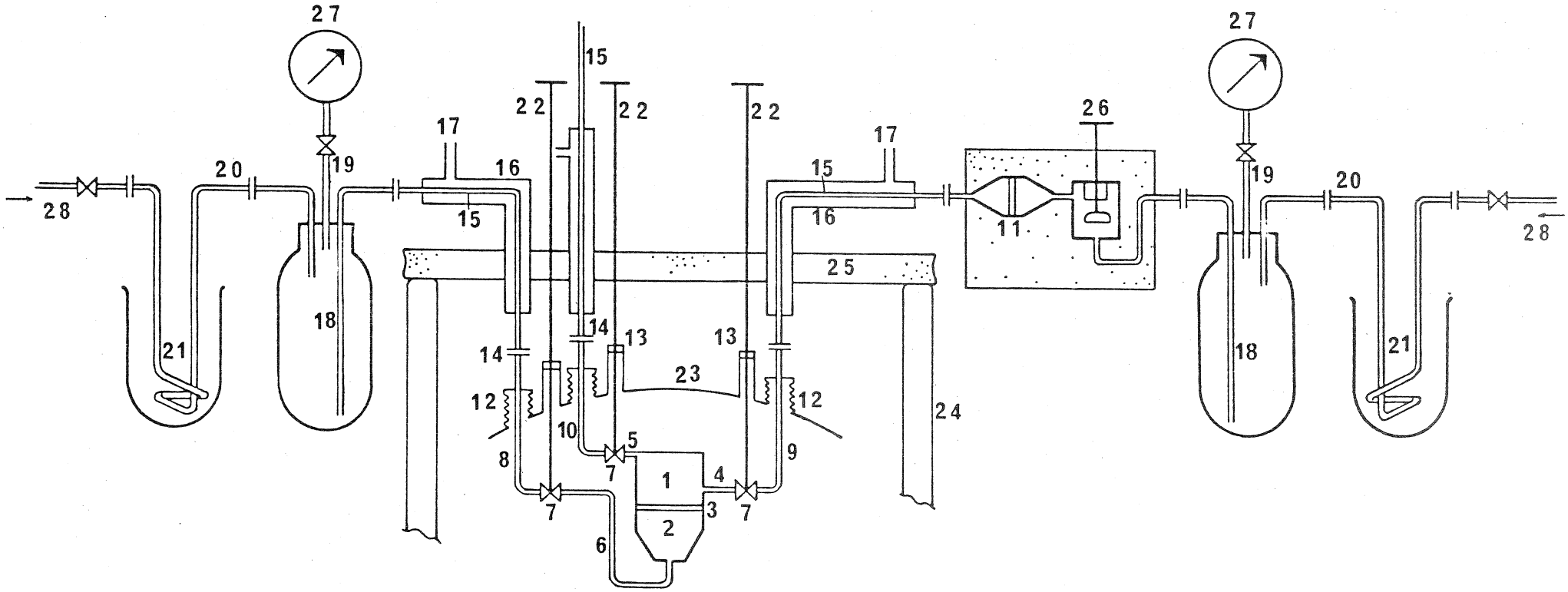

FIGURE 2.16 : SCHEMATIC LIQUID ARGON FILLING SYSTEM

NOTE: Legend for this figure is given in the following page

Legend for Figure 2.16

1. Top compartment
2. Bottom compartment
3. Diaphragm
4. & 5. Top liquid line (3.2 mm OD,1.8 mm ID,23 mm long)
6. Bottom liquid line (3.2 mm OD,1.8 mm ID,130 mm long)
7. Valve
8. Liquid line to bottom valve (3.2 mm OD,1.8 mm ID,27 mm long)
9. Liquid line to top middle valve (3.2 mm OD,1.8 mm ID,150 mm long)
10. Liquid line to top valve (3.2 mm OD,1.8 mm ID,170 mm long)
11. Filter
12. Brass bellows
13. Valve stem extension housing
14. Pipe coupling (Swagelok)
15. Inner liquid line (6.3 mm OD,4.3 mm ID)
16. Outer vacuum jacket (15.5 mm OD,13.5 mm ID)
17. Vacuum pump connection (9.5 mm OD,8.0 mm ID)
18. Liquid discharge line (6.3 mm OD,5.3 mm ID)
19. Vent line on flask (6.3 mm OD,5.3 mm ID)
20. Pressurant connection (6.3 mm OD,4.3 mm ID)
21. Argon liquefaction coil (6.3 mm OD,5.3 mm ID)
22. Cell valve extension stems (9.5 mm OD,8.0 mm ID)
23. Copper dome of cryostat
24. LN2 tank
25. Insulated suspension flange
26. Capsule breaker
27. Pressure gauge
28. Connection to argon gas cylinder

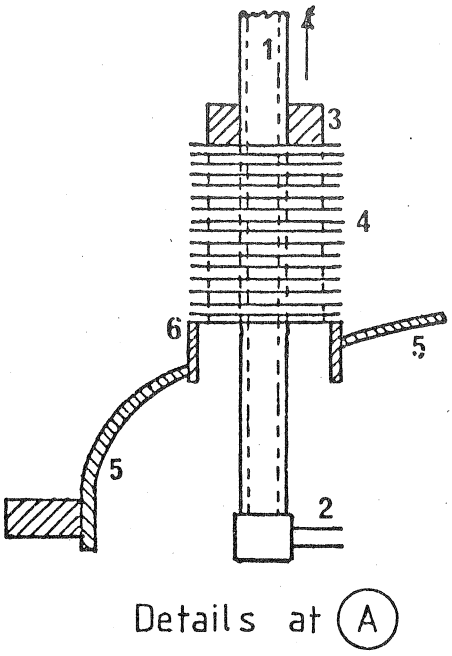

1. 6.5 mm OD . SS tube to flask
2. 3.2 mm OD SS tube to cell
3. Brass sleeve to couple (1) and (4)
4. Brass bellows
5. Copper dome
6. Brass mounting for bellows

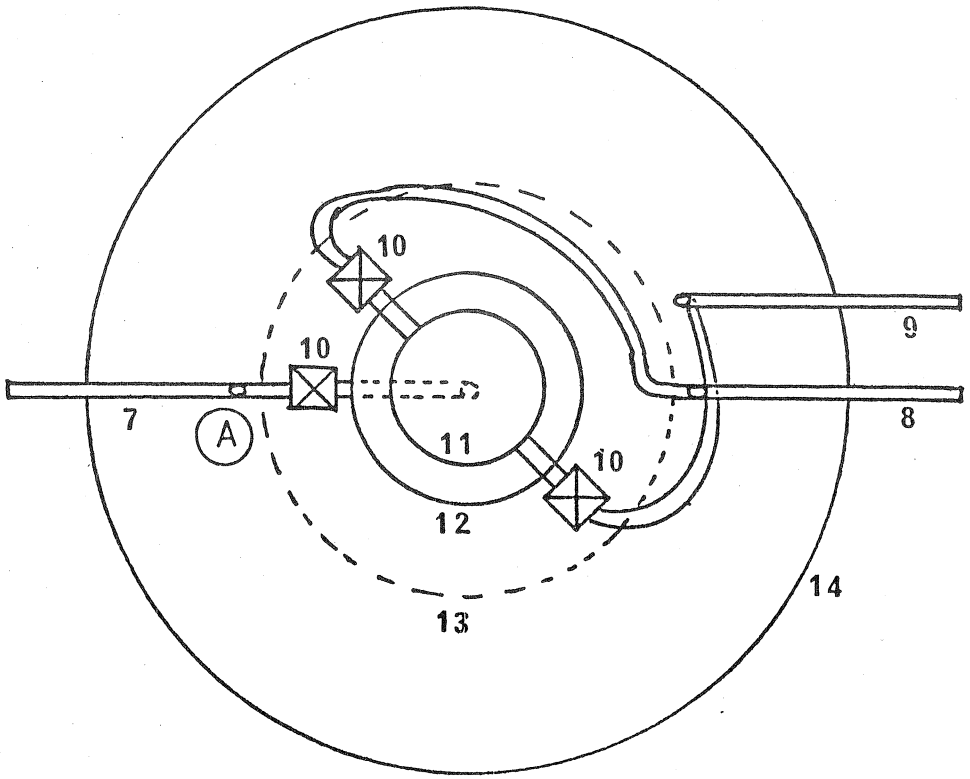

7. Liquid line (bottom)
8. Liquid line (top lower)
9. Liquid line (top - near light guide)
10. Cell isolation valves
11. Cell
12. Flange
13. Mean circle of rotating magnets
14. Copper vessel

FIGURE 2.17: LIQUID ARGON LINES INSIDE THE CRYOSTAT

of the cell. A capsule breaker was designed for this purpose (Figure 2.18). It consisted of a cradle to hold the capsule which had a breakable seal. The cradle could be pressed against the bottom of the stainless steel cup by turning the handle down. The assembly was made leak tight so that no radioactive tracer escaped from the unit. The assembly was insulated with polyurethane foam to prevent frost formation on the gland.

B. Purity of gas used in the study

Liquid argon was obtained by condensing the gas from high pressure cylinders supplied by Commonwealth Industrial Gases Pty. Ltd. in their standard 'G' size cylinders. The special grade argon had the following composition:

Purity	:	99.995%
Impurities		
Oxygen	:	less than 6 ppm
Nitrogen	:	less than 30 ppm
Carbon dioxide	:	less than 5 ppm
Hydrocarbons and methane	:	less than 1 ppm
Hydrogen	:	less than 1 ppm
Carbon monoxide	:	less than 1 ppm
Moisture at 15 C and full cylinder pressure	:	less than 12 ppm

Since argon was condensed in copper coil first and then transferred into the flasks, the impurities in the liquid actually used for the experiments could be expected to be reduced. Moisture was removed at two stages, namely in the silica gel drier and in the copper coil.

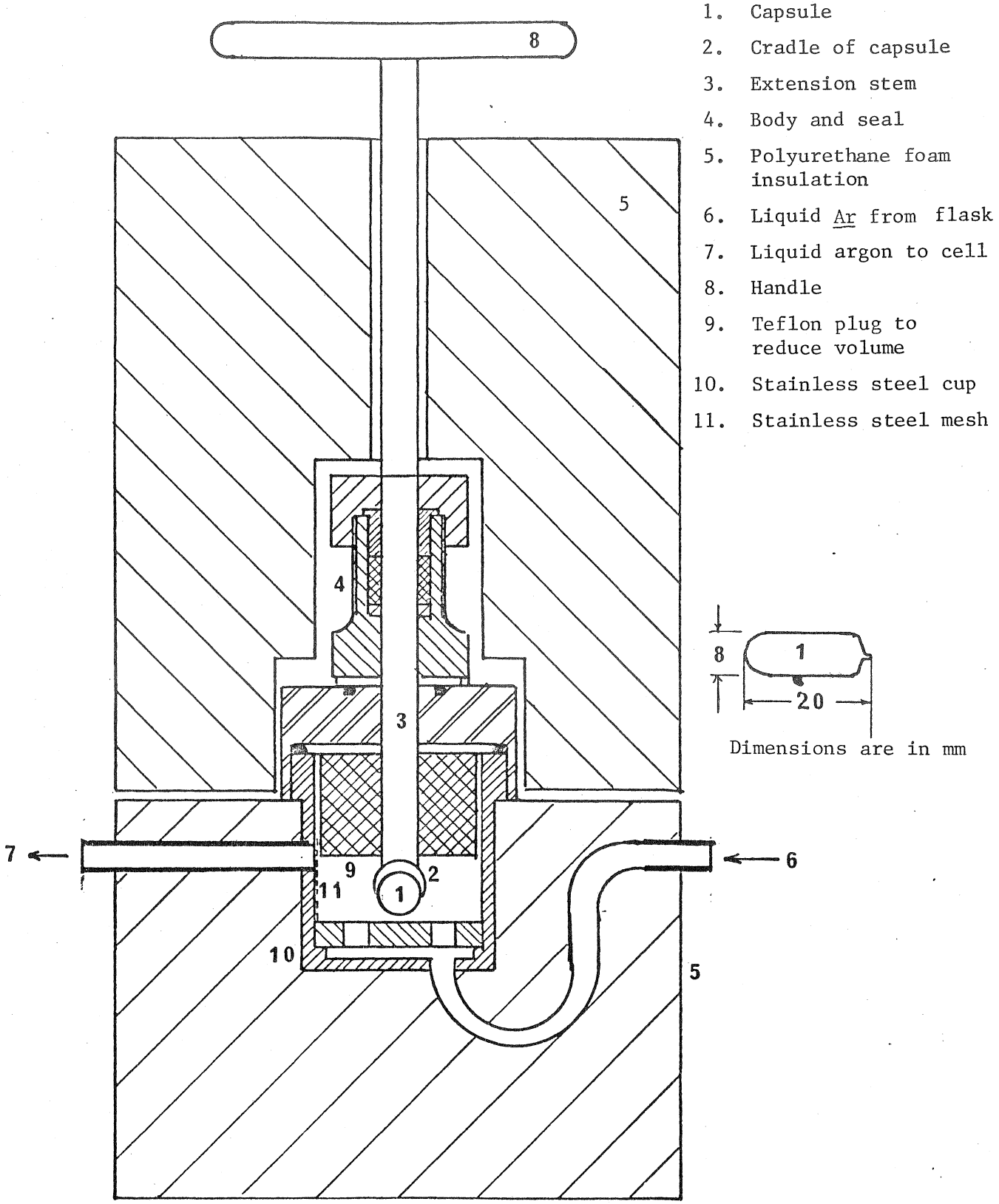

1. Capsule
2. Cradle of capsule
3. Extension stem
4. Body and seal
5. Polyurethane foam insulation
6. Liquid Ar from flask
7. Liquid argon to cell
8. Handle
9. Teflon plug to reduce volume
10. Stainless steel cup
11. Stainless steel mesh

Dimensions are in mm

FIGURE 2.18 : RADIOACTIVE TRACER CAPSULE BREAKER

2.2.5 Continuous monitoring system

The objective of the present study was to follow the diffusion of the Kr^{85} tracer in the cell using a continuous monitoring system thus avoiding the need to determine the concentrations separately in each of the compartments at the end of an experiment. The scintillation counting system was used since it is the easiest of the radioactive counting methods in the liquid state and it has a high efficiency and sensitivity (Fenyves and Haiman, 1969).

The scintillation counting system has the following subsystems: a) the scintillation crystal, b) the light guide, c) the photomultiplier tube assembly and d) the counting equipment. A schematic arrangement of the system is shown in Figure 2.19.

Although liquid argon itself is a scintillator (Kubota et al, 1978), a CsI crystal scintillator was employed to increase the efficiency of detection of radiation emitted by Kr^{85}. CsI was chosen in preference to NaI because of its non-hygroscopic nature and high efficiency for detection of β and γ rays at 100 K and below.

The purpose of the light guide was to transmit the photons emitted by the scintillator to the detection system. The light guide was made in two parts. The main part is shown in Figure 2.8. A conical transition piece was used at the top end to couple the light guide to the photomultiplier tube. The entire light guide unit was designed from optical considerations assuming that the total allowable variation in intensity across the photocathode should not be more than 2%. The height of the light guide was chosen as a compromise among the heat leak to the cell, the influence of the field due to the stirrer magnets on the performance of the photomultiplier tube and a reduction in intensity

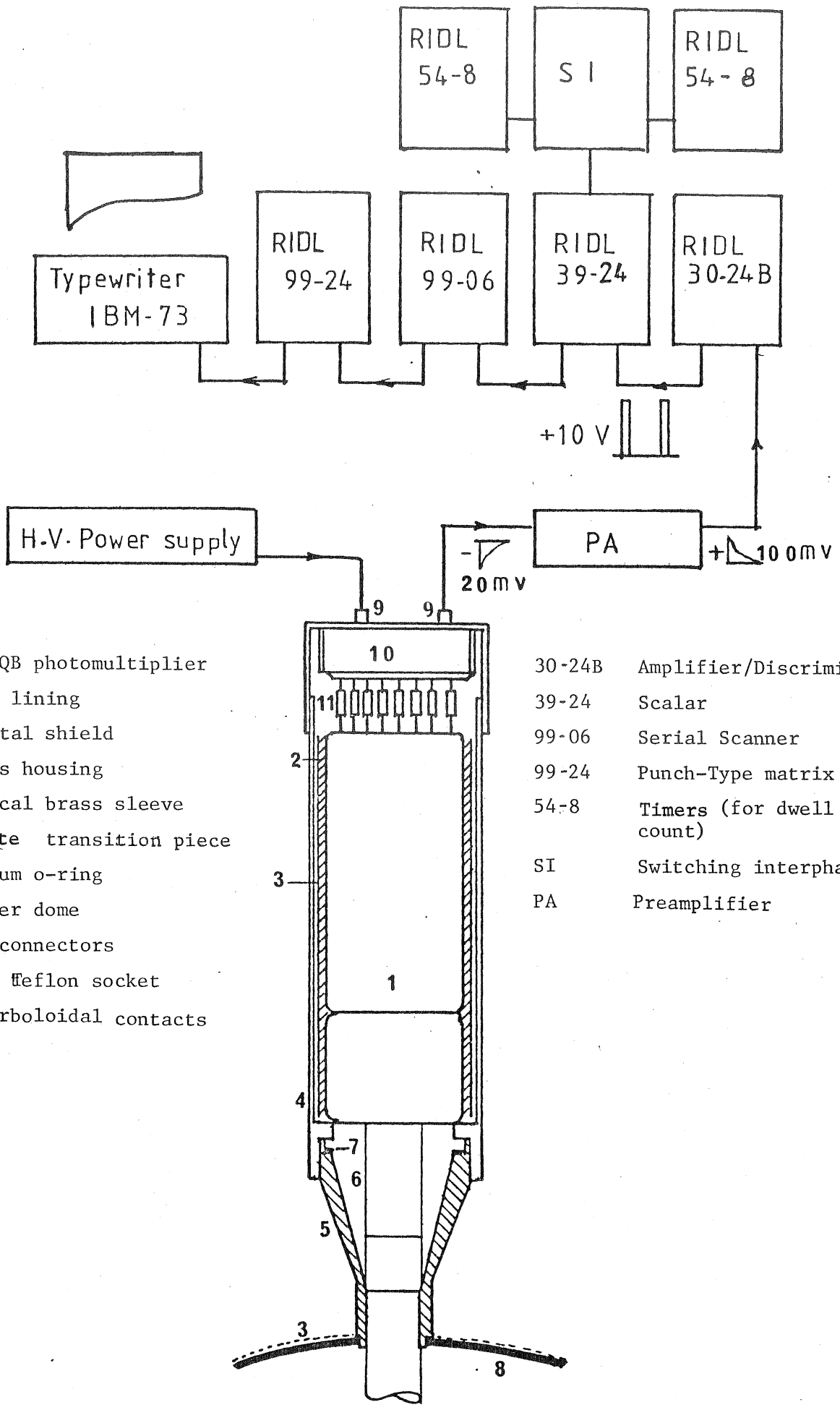

1. 9558QB photomultiplier
2. Felt lining
3. μ-metal shield
4. Brass housing
5. Conical brass sleeve
6. Lucite transition piece
7. Indium o-ring
8. Copper dome
9. BNC connectors
0. B19A Teflon socket
1. Hyperboloidal contacts

30-24B	Amplifier/Discriminator
39-24	Scalar
99-06	Serial Scanner
99-24	Punch-Type matrix
54-8	Timers (for dwell and count)
SI	Switching interphase
PA	Preamplifier

FIGURE 2.19: SCINTILLATION COUNTING SYSTEM

of photons at the photocathode (inverse square law).

An EMI 9558 QB photomultiplier tube was used. This tube was wrapped in a felt cushion and in a mu-metal shield. Hyperboloidal contacts were used to connect the pins to the EMI type B19A base. The entire assembly was housed in a light tight brass housing. This housing was positioned in the vapour space of the LN2 tank (Figure 2.3). It was observed that the housing of the tube cooled to about 170K which was sufficient to virtually eliminate the dark current.

The counting system comprises of a preamplifier, an amplifier-discriminator unit, the scalar and timer units and an interphase system to enable recording of the counting rate on an IBM electric typewriter. It was observed that the gain of the amplifier and the stability of the high voltage power supply were dependent on the ambient conditions. The entire apparatus was kept in an airconditioned room wherein the temperature was maintained at 20±1 C. Photographic plate 6 shows the photomultiplier tube and its components.

2.2.6 Suspension of the cell from the top dome

The thermal design of the cell required that the total heat leak to it should be less than a value which would disturb the thermal equilibrium beyond ±0.03 K. The sources of conduction heat leak to the cell were the lucite light guide, the argon valve extension stems, the liquid argon lines and the leads from the temperature sensors. The following heat balance equation can be written for the cell:

$$\Sigma\, m\, c_p\, dT/dt = \Sigma\, Q_1 - \Sigma\, Q_2 \qquad . \quad (2.1)$$

In the above equation m is the mass of the cell and its contents, c_p

the average specific heat of the cell assembly, T the temperature of the cell and Q the rate of heat transfer. Subscript 1 refers to heat transfer to the cell , 2 refers to heat transfer from the cell and Σ indicates summation due to all components. Table 2.1 gives a summary of the factors influencing the heat balance. The thermal model for the cell is shown in Figure 2.20. The quantities Q_1 and Q_2 may be positive or negative depending on whether the cell was colder or warmer than the environment. The cell lost heat by convection and radiation. This heat loss was partially compensated by the base heater, H1 (Figure 2.11).

The liquid nitrogen level and the shape of the top dome were chosen such that a non-uniform temperature distribution existed on the dome. Through trial and error and experimentation it was possible to attain a condition whereby the temperature of the dome at the centre (where the light guide passes through it) was nearly the same as that of the cell. Consequently, the heat conduction through the light guide could be minimised. The anchoring points for the liquid lines and the valve stems were obtained by providing extensions from the dome. The valve stem anchoring can be seen in Figure 2.1. The stainless steel tubes around the stem were made thin and long to reduce conduction heat leak. This material was an obvious choice because of its low thermal conductivity and high strength. It was also necessary to ensure that these extensions did not contribute too much to the gas volume of the cryostat.

Anchoring of the liquid argon lines posed no problems as their length in the gas volume could be increased. However, it was necessary to ensure that argon did not freeze in the line where it enters the cryostat. Referring to Figure 2.17, the bellows arrangement provided enough resistance to conduction heat leak from the argon line to the copper dome.

TABLE 2.1: HEAT BALANCE COMPONENTS (EQUATION 2.1)

(Reference Figure 2.20)

Left hand side		Right hand side		
$(\sum_{Cell} m\ c_p)\ \frac{dT}{dt}$	=	ΣQ_1	-	ΣQ_2
Components: i) mass of cell and its components ii) liquid argon $\frac{dT}{dt}$ = 0.06 K / cycle (Figure 2.20)		Components: i) Conduction due to anchoring . Light guide(Q1P) . Valve stem (3 Q1V) . Liquid lines(3 Q1L) . Instrument leads (24 Q1W) ii) Enthalpy of GN2 flow in $(\dot{m}\ c_p\ T)_{GN2\ in}$ iii) Heater H1		Components: i) Convection heat transfer from cell $(\sum_{cell} h\ A)\ \Delta T$ $\Delta T = T_{cell} - T_{GN2\ bulk}$ ii) Enthalpy of GN2 flow out $(\dot{m}\ c_p\ T)_{GN2\ out}$ iii) Radiation between cell and copper vessel

Notes: 1. $T_{GN2\ bulk}$ is determined by enthalpy of GN2 in the cryostat, enthalpy of GN2 flowing in and out.

h is the heat transfer coefficient, A the surface area and $\dot{m}$ the mass flow rate

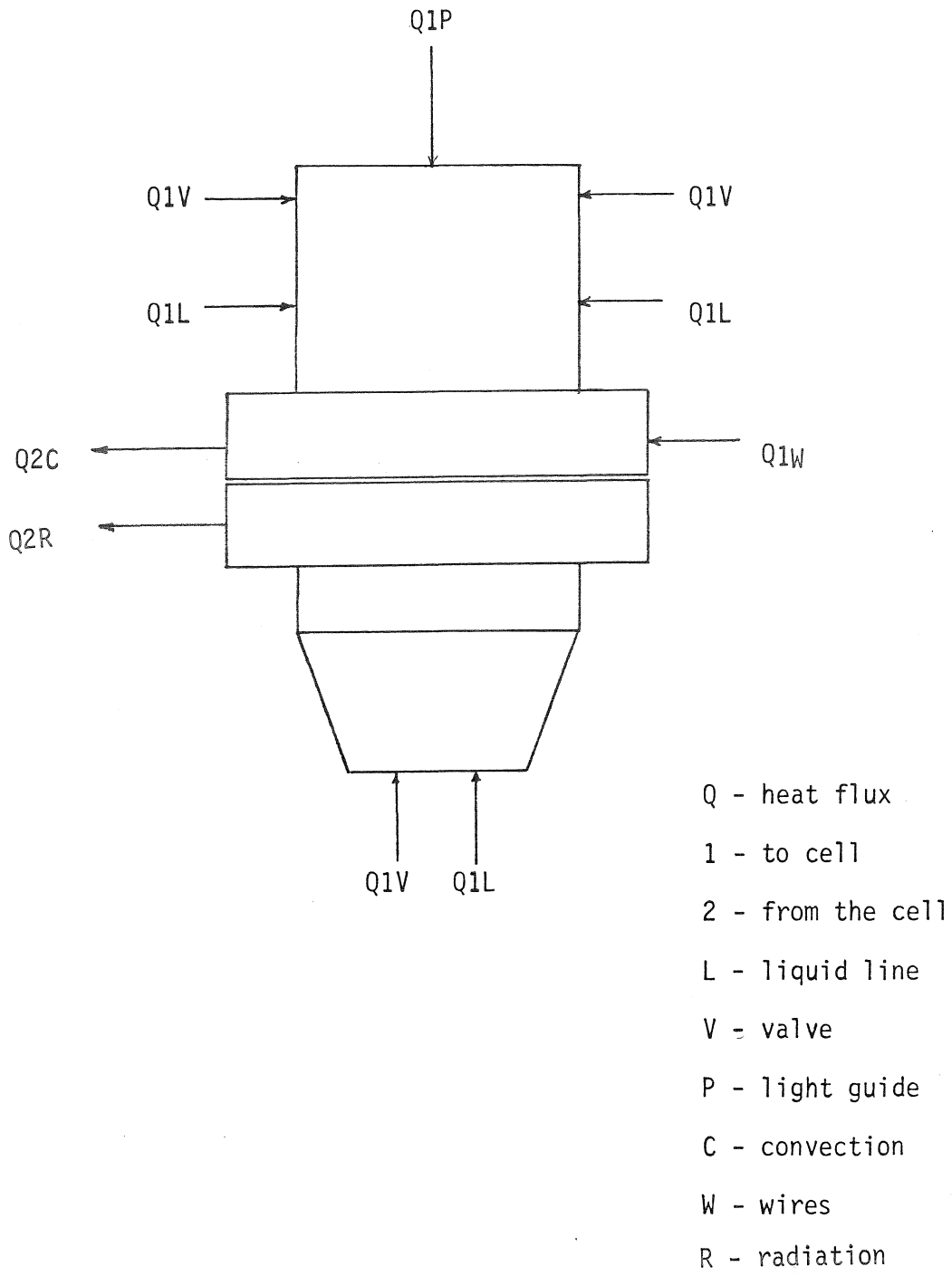

FIGURE 2.20 : CELL MODEL FOR HEAT BALANCE

In the case of instrument leads, the wires were made as long as 200 mm and a major portion remained in the gas volume. All the leads were taken out through one port which was made leak tight by potting it with Sylgard 184. The arrangement is shown in Figure 2.21.

Photographic plate 7 shows the suspension of the cell from the top dome and suspension of the dome from the sandwich flange.

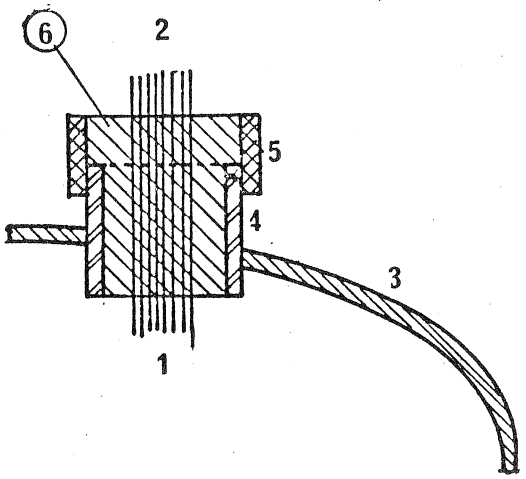

FIGURE 2.21: FEEDTHROUGH FOR WIRES

1. Leads from cell
2. Leads to instruments
3. Copper dome
4. Brass bush
5. Teflon cup
6. Sylgard potting

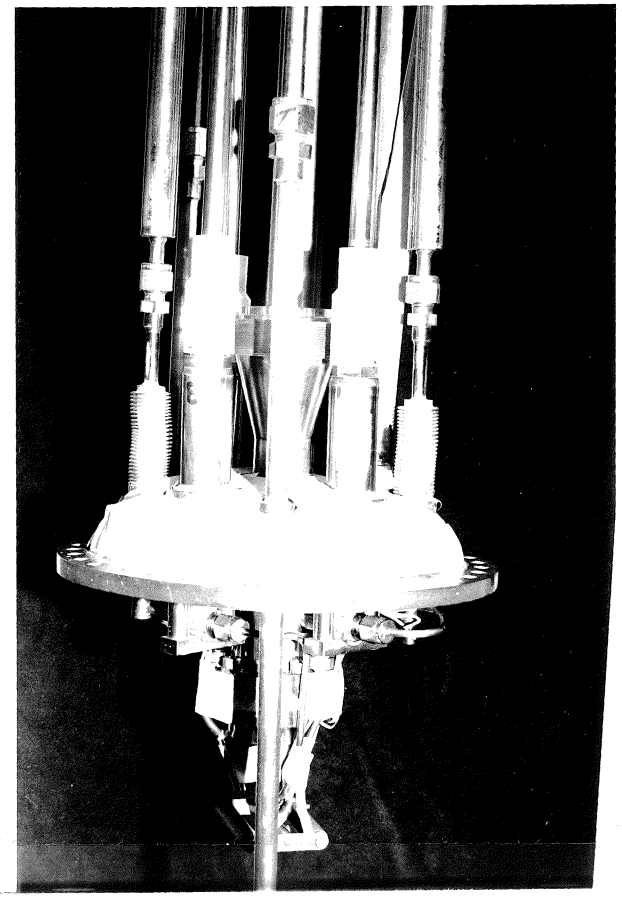

a. SUSPENSION SYSTEM ABOVE THE DOME

b. SUSPENSION OF DOME FROM THE SANDWICH FLANGE

PLATE 7

3. MATHEMATICAL TREATMENT

In this chapter the equations from which the diffusion coefficient can be determined are derived. The procedure adopted for data processing is also included. The normal diaphragm cell equations have been detailed by Mills and Woolf (1968). For the case of a continuously monitored diaphragm cell, the data are in the form of counting rate (which is proportional to the concentration) due to the radioactive tracer in one of the compartments (in this case the top) as a function of time.

3.1 Equations of Diaphragm Cell

For a gradient filled diaphragm, the diffusion coefficient can be calculated using the equations given below (Mills and Woolf, 1968):

$$D = \frac{1}{\beta t} \ln \left[\frac{{}^{o}C_T - {}^{o}C_B}{C_T - C_B} \right] \quad , \quad (3.1)$$

where

$$\beta = \frac{A_c}{\ell} \left(\frac{1}{V_T} + \frac{1}{V_B} \right) \left(1 - \frac{\lambda}{6} \right) \quad , \quad (3.2)$$

D is the diffusion coefficient, β is the cell constant, A_c is the effective cross-sectional area available for diffusion, ℓ is the length of the diffusion path, t is the time of a diffusion experiment and C is the concentration. Suffixes o, T, B and D refer to initial condition, the top compartment, the bottom compartment and the diaphragm respectively. λ is equal to $2V_D/(V_T+V_B)$.

In the present study it was assumed that a linear gradient exists across the diaphragm. It is a reasonable assumption if the starting time for a diffusion experiment is reckoned from a time when the gradient has been established.

3.2 Modifications for the Case of Continuous monitoring

The radioactive tracer was introduced into the top compartment of the diaphragm cell and its diffusion was monitored using the radiochemical counting equipment. The counts given by the scintillation counter are directly proportional to the concentration of the tracer in the top compartment. Thus, the concentration C_T was known as a function of time. In the absence of information about C_B, equation (3.1) has to be modified to suit the present experimental conditions.

From the law of conservation of mass, when the cell was isolated, we have

$$(V_B+0.5\ V_D)\ {}^{o}C_B + (V_T+0.5V_D)\,{}^{o}C_T = (V_B+0.5V_D)\ C_B + (V_T+0.5V_D)\,C_T \quad . (3.3)$$

Equation (3.1) can be rewritten as

$$C_T - C_B = ({}^{o}C_T - {}^{o}C_B)\ \exp(-D\,\beta t) \quad . (3.4)$$

Using the above two equations, the quantity C_B can be eliminated and an equation can be obtained relating C_T with other quantities. The resulting equation is given below:

$$\boxed{C_T = A + B \exp(-bt)} \quad , (3.5)$$

where
$$A = \left(\frac{V_T+0.5V_D}{V_B+V_T+V_D}\right) {}^{o}C_T + \left(\frac{V_B+0.5V_D}{V_B+V_T+V_D}\right) {}^{o}C_B \quad , (3.6)$$

$$B = \frac{({}^{o}C_T - {}^{o}C_B)\ (V_B+0.5V_D)}{V_B+V_T+V_D} \quad , (3.7)$$

and
$$b = D\beta \quad . (3.8)$$

Equation (3.5) relates the counting rate due to the tracer in the top compartment and time. The constants A, B and b are independent of time. The diffusion coefficient D is contained in the constant 'b' through the equation (3.8). The cell constant β was obtained through a calibration experiment (described in Chapter 4).

3.2.1 Choice of starting time for experiments

Equation (3.3) is written for an arbitrary starting time. Varying the starting time would only alter the values of $^{o}C_{T}$ and $^{o}C_{B}$ and hence the constants A and B. However, the constant 'b' remains unaffected by the choice of starting time. Further it can be shown that

$$-b = (\partial^2 C_T/\partial t^2)/(\partial C_T/\partial t) \qquad . (3.9)$$

Equation (3.9) proves that the constant 'b' is only a function of differentials of the counting rate with respect to time.

3.2.2 Advantages of continuous monitoring

From the foregoing section it can be seen that it is not necessary to know the exact starting time of an experiment if the method of continuous monitoring is adopted. To determine the diffusion coefficient , ideally, it is sufficient if the counting rates at three instants are known . . . The method of continuous monitoring eliminates the errors associated with sampling of the contents of the top and the bottom compartments at the end of an experiment, their dilution and counting. The sources of error for the case of continuous monitoring are limited to: a) the calibration error, b) the counting error during monitoring and c) the error in the mathematical processing of data to determine the constant 'b'.

If an experiment is not progressing properly, for example, due to the presence of bulk flow, it is possible to observe such discrepencies during an experiment, whereas it would be impossible to do so in a normal diaphragm cell experiment.

It is not necessary to know exactly, the background counting rate as long as it is reasonably constant. The effect of the background counts is automatically absorbed in the constant A of equation (3.5). Consequently, it is possible to operate the counting system under a low signal to background ratio.

3.3 Data Processing

The data are in the form of counts per minute as a function of time. To obtain values of the constants A,B and b several sets of data were used to fit a curve of the type given by equation (3.5). A weighted non-linear least squares method was used for this purpose (Buckingham, 1957). The details of the method are given in Appendix - I.

3.4 Treatment of the Cell Constant

The cell constant given by equation (3.2) was obtained through a calibration experiment at room temperature. However, one should expect the cell constant to change when the cell is cooled to cryogenic temperatures. Therefore, it is necessary to estimate the value of the cell constant at such temperatures. Using the thermal contraction relations for length, area and volume, equation (3.2) can be rewritten to give an equation for the cell constant at low-temperatures (LT), which is as follows:

$$\beta_{LT} = \frac{A_c\,(1-2\alpha\,\Delta T)}{\ell\,(1-\alpha\,\Delta T)}\left[\frac{1}{V_T}+\frac{1}{V_B}\right]\left[\frac{1}{(1-3\alpha\,\Delta T)}\right](1-\frac{\lambda}{6}) \quad . \quad (3.10)$$

The above equation can be simplified as follows:

$$\beta_{LT} = \frac{(1-2\alpha\,\Delta T)}{(1-\alpha\,\Delta T)(1-3\alpha\,\Delta T)}\,\beta \qquad .(3.11)$$

In the above equation α is the coefficient of thermal contraction for the material of the sinter. Assuming that the calibration was performed at 298.15 K and using a value of $\alpha\,\Delta T = 0.28 \times 10^{-2}$ for stainless steel when cooled from 298.15 K to 90 K (Wigley and Halford, 1971)

$$\beta_{LT} = 1.00564\ \beta \qquad .(3.12)$$

The above relation was taken into consideration for calculating the diffusion coefficient from equation (3.8). The value used in that equation was β_{LT} and not β at room temperature.

4. EXPERIMENTAL PROCEDURES

In this chapter the experimental procedures for measurement of diffusion coefficients are described. It covers the preliminary operations such as calibration and obtaining the necessary settings on the instruments, the cool-down process and actual diffusion experiments.

4.1 Calibration Procedures

The components of the apparatus that needed calibration were the diaphragm cell and the temperature sensors.

4.1.1 Calibration of the diaphragm cell

The cell constant (β) needs to be determined. Reliable diffusion data are lacking for liquids which could be used in the temperature range of 85 - 103 K. Consequently, the cell constant was obtained using diffusion data for benzene and water at 25 C and correcting the value of β for use at low-temperatures as described in Section 3.4. The calibration procedure also involved determination of the volumes of the top and the bottom compartments and the sintered stainless steel diaphragm. The following table gives the values of diffusion coefficients used for the purpose of calibration.

TABLE 4.1 : DIFFUSION DATA FOR CALIBRATION LIQUIDS AT 25 C

Tracer	Bulk liquid	D x 10^5 (cm^2/s)	Reference
$^{14}C_6H_6$	Benzene	2.207±0.003	Collings and Mills (1970)
HTO	Water	2.236±0.004	Mills (1973)

A lucite cell was fabricated which had a geometry identical to the actual diffusion cell except that the former did not have the opening for the light guide. Using this cell the volume of the diaphragm was determined following the procedures recommended by Mills and Woolf (1968) and McCool (1971). Due to usage over prolonged periods of a year and more and due to continuous cycling of the diaphragm between temperatures of 85 and 300 K for each cool-down and warm-up, it was observed that its volume was affected marginally. However, this was found to be less than 5% during the period of present study. Even an uncertainty of 10% did not affect the final value of the cell constant beyond a fraction of a percent. During the measurement of diaphragm volume, the reproducibility was about 3%.

The volumes of the compartments of the actual cell were determined using the standard diaphragm cell procedures (Mills and Woolf, 1968). The stainless steel diaphragm cell was calibrated using benzene as the bulk liquid. As a second check the same cell was used to determine the diffusion coefficient of water with HTO as tracer. The value obtained was found to be within 2% of the data reported by Mills (1973). Both the experiments were conducted at 25 C. For the purpose of calibration the actual light guide assembly was replaced with an identical teflon piece and a glass window.

The value of A_c/ℓ for the diaphragm could be obtained from a knowledge of the cell constant. However, before each assembly of the cryostat the cell constant was checked using the lucite cell and water as the calibration liquid. Table 4.2 gives details of calibration of the cell.

TABLE 4.2 : DETAILS OF CALIBRATION OF THE CELL AT ROOM TEMPERATURE

Date	Cell	V_D cm^3	V_B cm^3	V_T cm^3	A_c/ℓ cm	β cm^{-2}
Sep 78	Lucite	0.404	24.7192	28.1412	4.880	0.3650
Apr 79	Lucite	0.419	25.1399	28.5559	4.910	0.3615
Jun 79	Actual	0.403	23.0448 to 22.6991	25.3658 to 25.2438	4.887	0.3958 to 0.4042
Jan 80	Lucite	0.387	24.4367	27.8775	4.863	0.3680

A. Uncertainty in the calibration of the cell

The uncertainty in the calibration is due to the volume of liquid argon lines. The calibration of the cell was made prior to fixing the liquid lines. It was not clear whether the liquid line volumes (which are 0.346 cm^3 and 0.122 cm^3 for the bottom and the top compartments respectively) form a part of the cell volume. The cell constants without a liquid line contribution and with a liquid line contribution differ by about 1%. In the present study the cell constant was taken as the average of these two values and was 0.4023 cm^{-2} when corrected for low temperature operation.

All the tracer diffusion data for Kr^{85} in liquid argon were obtained between June and December 1979. The calibration before and after this schedule of experiments showed that the cell constant remained within 1% of the stated value. Considering the other uncertainties such as the purity of the liquids used and the data for calibration liquids it is expected that the cell constant is accurate to ±1%.

4.1.2 Calibration of temperature sensors

A. Platinum Sensors

A set of three platinum resistance thermometers was calibrated by National Measurement Laboratory, Lindfield, NSW. The range of calibration was 85 - 150 K. One of the sensors was used as a secondary standard for subsequent calibrations. One was mounted on the top compartment of the cell. The third one was retained as a spare to substitute either of the earlier ones in the event of their non-performance.

Prior to each assembly the sensors were checked for their accuracy of temperature measurement. For this purpose, the boiling points of nitrogen, argon and oxygen at atmospheric pressure and the ice point were used as reference points. The calibration was performed against the secondary standard platinum resistance thermometer. Over a period of usage a marginal change was observed. The calibration curve for the sensors was obtained in accordance with the procedure laid down by IPTS68 (amended edition of 1975) as given by Kemp (1977).

B. Thermocouples

Copper-constantan thermocouples (Type T) were also calibrated at the secondary reference points mentioned above, with liquid nitrogen as reference bath. Since thermocouples were used only as a guide to assessment of temperature uniformity of the cell, no elaborate corrections were applied to the calibrated values. However, it must be mentioned that the temperature of the reference bath crept up steadily due to condensation of air. Precautions were taken to replenish the reference bath with a fresh supply of liquid nitrogen. It was also necessary to correct for the boiling point of nitrogen due to daily

variations of atmospheric pressure in Canberra. It was observed that the net effect was to induce an uncertainty of 8 μv in thermo-emf which corresponds to about 0.5 K. Since the thermocouples were no more accurate than 0.5 K(the specification of the supplier) the above procedure was assumed to be satisfactory.

The details of platinum sensor settings for resistance and the thermocouple outputs with LN2 reference bath are given in Table 4.3 at temperatures of interest in this study.

4.1.3 Settings on the temperature control system

The Artronix temperature controller has a 10 turn dial setting to obtain the required resistance which corresponds to the reference temperature about which control is desired. The settings were obtained by calibrating the TEMP SET dial for bridge balance against a given resistance which can be set on a high precision decade box. The gain of the Artronix controller was set such that the recorder ouput (which is proportional to the deviation from the set point) was about 15 mv/0.01 ohm (about 0.023 K). The controller was operated on manual mode only.

The emphasis was on limiting the fluctuations in temperature to less than 0.03 K. It was decided to opt for high frequency low amplitude cycling as shown in Figure 2.13(c). This type of control is characterised by an offset, which was compensated by setting the resistance on the L & N bridge 0.01 or 0.02 ohm higher than the required resistance. An appropriate adjustment of the threshold and hysteresis were necessary.

4.1.4 Settings on the counting system

The cathode to anode voltage of the photomultiplier

TABLE 4. 3 AVERAGE SETTINGS ON THE TEMPERATURE CONTROL SYSTEM

T (K)	Required resistance(Ω)		Artronix setting on range 2	L & N Bridge setting (Ω)	Preheater coil		GN2 valve opening (i)	Thermocouple output for LN2 reference bath μv
	BPRT	TPRT			I D (cm)	approx. length(cm)		
85.00	23.72	23.72	268	23.73	0.18	14	70	138
86.00	24.15	24.15	290	24.16	0.18	14	100	156
89.30	25.56	25.56	360	25.57	0.40	90	150	214
93.30	27.25	27.25	440	27.26	0.40	90	160	287
96.00	28.37	28.37	490	28.39	0.40	90	125	337
100.00	30.09	30.08	563	30.10	0.40	90	270	414
103.00	31.36	31.36	615	31.37	0.40	90	160	472

(i) Valve opening in degrees from fully closed position

Note: Threshold on the thermal discriminator was set to 70 mv for all experiments

tube, the amplifier gain and the discriminator settings in the counting equipment were arrived at after conducting a series of tests by counting Cs^{137} and Kr^{85} at room temperature and cryogenic temperatures respectively. The settings so chosen resulted in the maximum signal to background ratio. Prior to conducting actual diffusion experiments the stability of the entire system was thoroughly tested over a period of several days.

4.2 Cool-down of the Cryostat

The quartz window of the photomultiplier tube was very sensitive to sudden changes in temperature. To avoid any thermal stresses on this component the cryostat was cooled down at a rate not exceeding 10 K/hr. The cool-down of the cryostat was monitored through the thermocouples mounted on the cell and the outer surface of the brass housing of the tube. Liquid nitrogen was pumped into the tank using the pressurised transfer method at intervals varying between 90 and 30 min to achieve a cooling rate specified earlier. The cell and the copper vessel were flushed with gaseous argon and nitrogen respectively at frequent intervals to prevent the ambient air from being sucked in. A typical cool-down curve is shown in Figure 4.1. It was ensured that the entire cell cooled as a single unit.

4.3 Diffusion Experiments

The procedure associated with an actual experiment involved the following operations: a) loading the cell with liquid argon and introducing the tracer into the top compartment, b) monitoring the diffusion of the tracer over a period of 2 to 3 days, and c) termination of the experiment.

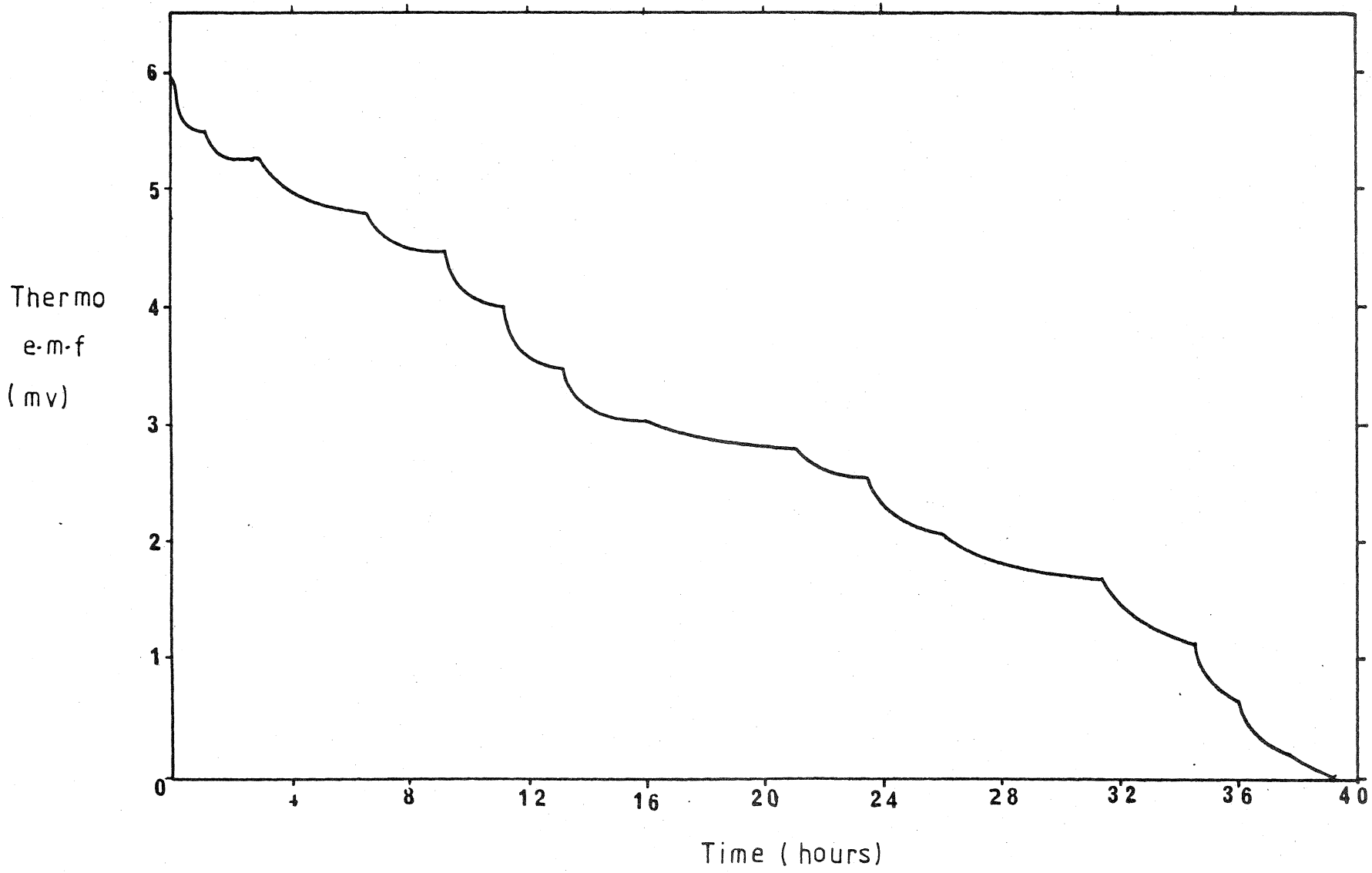

FIGURE 4. 1 : A TYPICAL COOL-DOWN CURVE FOR THE CRYOSTAT

A. Loading the cell

The diaphragm cell was flushed clear of any residual gas before the diffusion experiment was commensed. The piping arrangement for condensing and transferring liquid argon is shown in Figure 2.16. Figure 4.2 shows a simplified system which forms the basis for further description. Valves V_{BC} and V_{T2} were closed and the Swagelok connector JB was removed. Gaseous argon was allowed to pass from the high pressure cylinder via the drier, the filter, V_{TC}, the cooling coil, the flask ART, the capsule breaker, valve V_{T1}, the cell and the valve V_B. The gas would escape at JB into the atmosphere. This operation enabled flushing of the cell. V_{BC} and V_{T2} were opened and the joint JB was made tight. After flushing the cell in this mode for a few minutes valves V_{T1}, V_{T2} and V_B were closed isolating the cell. The gauges P2 and P3 were disconnected and the valves V_{BV} and V_{TV} opened. The liquefaction coils were immersed in baths of liquid nitrogen. Liquid argon would be collected in the flasks ART and ARB.

The following procedure was followed for loading the cell. The gauges P2 and P3 were connected. V_{T2}, V_B and V_{BC} were opened and V_{TC} was closed. Argon from the cylinder was used to pressurise the vapour space in the flask ARB and to transfer liquid argon into the cell. The cell filled after cooling down of the lines was complete. V_{T2}, V_B and V_{BC} were closed. V_{TC}, V_{T1} and V_{T2} were opened. This operation aided pressurising the vapour space of the flask ART and transferring liquid argon into the top compartment of the cell. During this operation, firstly the volume of liquid above the liquid entry line in the top compartment was expelled and then after cool-down of the transfer line the volume was refilled with liquid from the flask ART. While the transfer was still in progress the capsule containing the

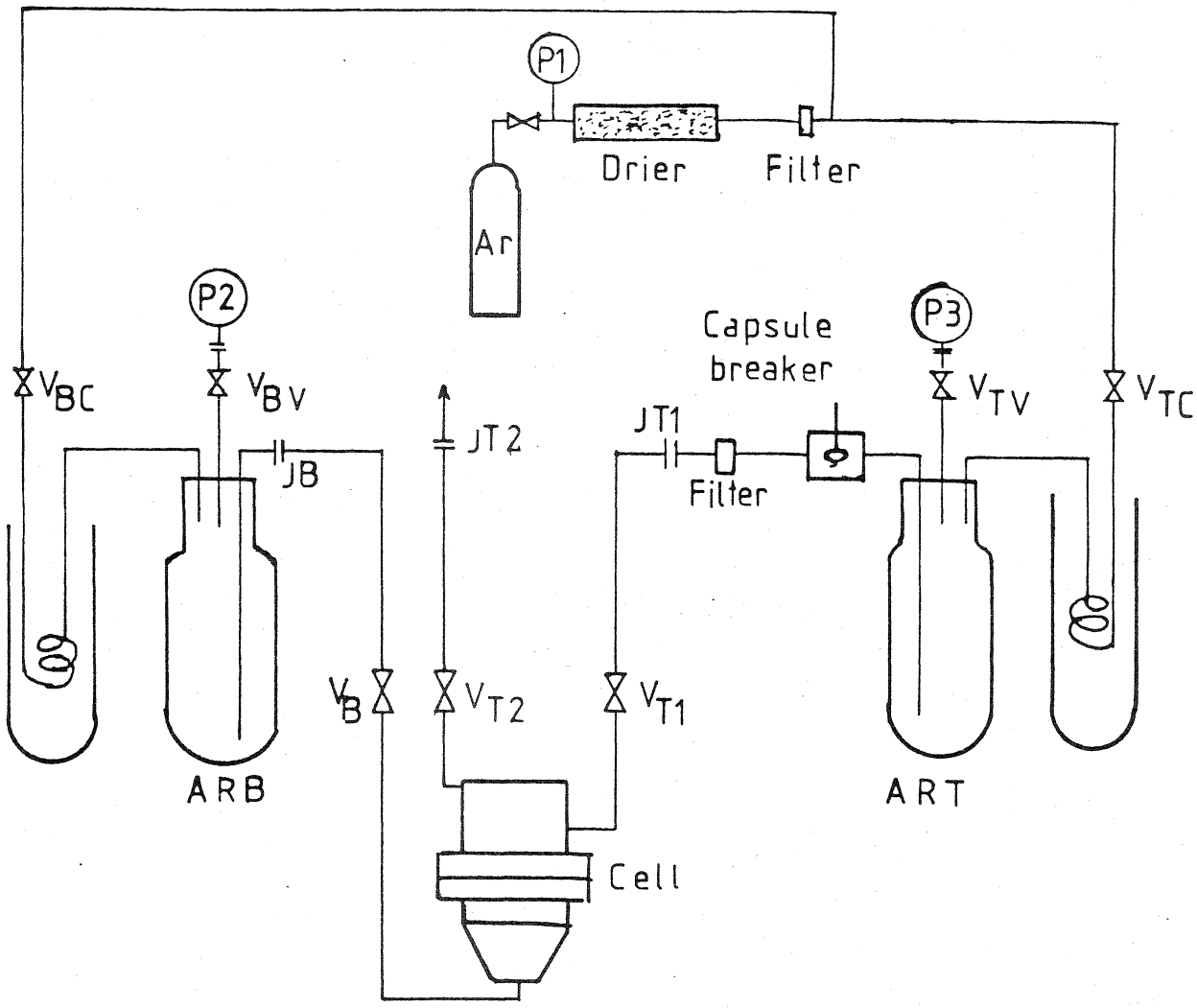

FIGURE 4.2 : SCHEMATIC LIQUID ARGON AND TRACER LOAD SYSTEM

radioactive tracer (Kr^{85}) was broken and the valve V_{T2} was closed after 8 to 12 seconds. This time delay was necessary to ensure that the slug of tracer had entered the top compartment of the cell. The entire filling operation resulted in causing some disturbances to the thermal equilibrium of the cell. The cell was cooled down to the set temperature while the pressure was retained on the flask ART. The valve V_{T1} was closed only when the thermal equilibrium was attained at the operating temperature. The transfer pressures on the flasks were chosen such that they were atleast 1 bar above the saturation pressure corresponding to the operating temperature. This was necessary to ensure that the entire cell volume was filled with liquid argon and that no vapour pockets were trapped in the cell.

B. Diffusion experiment

While thermal equilibrium was reached within 30 minutes after introducing the tracer, the counting rate was found to stabilize only after 8 to 12 hours. For this reason the starting time of the diffusion experiment was reckoned after the counting rate had stabilized. The duration of an experiment ranged from 2 to 3 days. It was pointed out in Chapter 3 (Section 3.2.2) that in the case of continuous monitoring it is not necessary to know the starting time.

The counting rate was recorded using an IBM electric typewriter. The temperature fluctuations of the top and the bottom compartments were monitored using a chart recorder. Periodically, the thermocouple outputs were measured using a Solartron A200 digital voltmeter to cross-check the temperature uniformity of the cell. It was observed that there were no detectable gradients larger than 0.03 K in magnitude. The LN2 and GN2 source dewars were replenished at intervals of 24 hours. Two sets of identical dewars with transfer systems were

retained in the laboratory so that the change could be effected with minimum disturbance to temperature uniformity.

C. Termination of an experiment

At the end of an experiment to verify that there were no leaks from the cell, the bottom compartment was connected to a pressure gauge and the valve V_B was opened. If the cell were full of liquid the gauge would read saturation pressure corresponding to the operating temperature. This was found to be true for all the experiments. The cell was then flushed with gaseous argon as described earlier.

Appendix - III presents the details of a typical diffusion experiment.

5. RESULTS

In this chapter are given the results of tracer diffusion coefficients for krypton in liquid argon measured in the temperature range of 85 -103 K. A discussion of the results is made in the next chapter.

The variation of counting rate with time as given by the counting apparatus and the temperature corresponding to the experiment form the primary data. The plot of ln (C-A) against time (t) forms the secondary data. For each experiment the plots obtained are similar to the ones shown in Figure A 3.1 (Appendix - III).

A summary of . tracer diffusion coefficients for krypton in argon with error limits is given in Table 5.1. The numerical accuracy of various parameters will be discussed in the next chapter. The Arrhenius plot (ln D_{Kr} vs T^{-1}) is shown in Figure 5.1. For the sake of comparison the results of Cini-Castagnoli and Ricci (1960) are superposed in this figure.

From the present experimental results , tracer diffusion coefficients of krypton in argon are found to fit the following relation:

$$D_{Kr} = 55.85 \exp(-304.6/T) \times 10^{-5} \quad cm^2/s \quad . \quad (5.1)$$

Over a temperature range of 85.4 to 90.2 K the experimental data of Cini-Castagnoli and Ricci (1960) can be represented by the following equation:

$$D_{Kr} = 52.5 \exp(-312/T) \times 10^{-5} \quad cm^2/s \quad . \quad (5.2)$$

TABLE 5.1: EXPERIMENTAL TRACER DIFFUSION DATA FOR KRYPTON IN ARGON

T (K)	Run ID	P (bar)	ρ (g/cm^3)	$Dx10^5$ (cm^2/s)	1 %	2 %	3 %
85.00	SEP 3	3.5	1.4085	1.552	4.0	1.5	4.4
85.00	JUL27	1.2	1.4078	1.641	7.2	2.9	7.8
86.00	SEP20	4.3	1.4027	1.561	3.6	3.0	4.8
86.00	JUL10	1.2	1.4017	1.647	6.4	3.0	7.1
89.30	NOV22	3.1	1.3821	1.930	2.8	2.3	3.8
89.30	SEP 9	4.0	1.3824	1.756	3.7	0.6	3.9
93.30	DEC 8	3.8	1.3569	1.942	1.3	0.8	1.8
93.30	DEC 3	3.1	1.3566	2.086	2.8	2.8	4.1
96.00	OCT22	4.8	1.3396	2.361	2.5	1.1	2.9
96.00	OCT27	4.8	1.3396	2.426	1.6	1.5	2.4
100.00	NOV 5	4.9	1.3124	2.664	2.6	2.4	3.7
100.00	DEC12	4.3	1.3121	2.708	1.3	1.4	2.2
103.00	NOV18	5.6	1.2915	2.921	1.1	0.4	1.5
103.00	NOV12	4.8	1.2911	2.917	1.3	0.4	1.7

Note: 1. Uncertainty in 'b'

2. Scatter in 'b'

3. Overall uncertainty

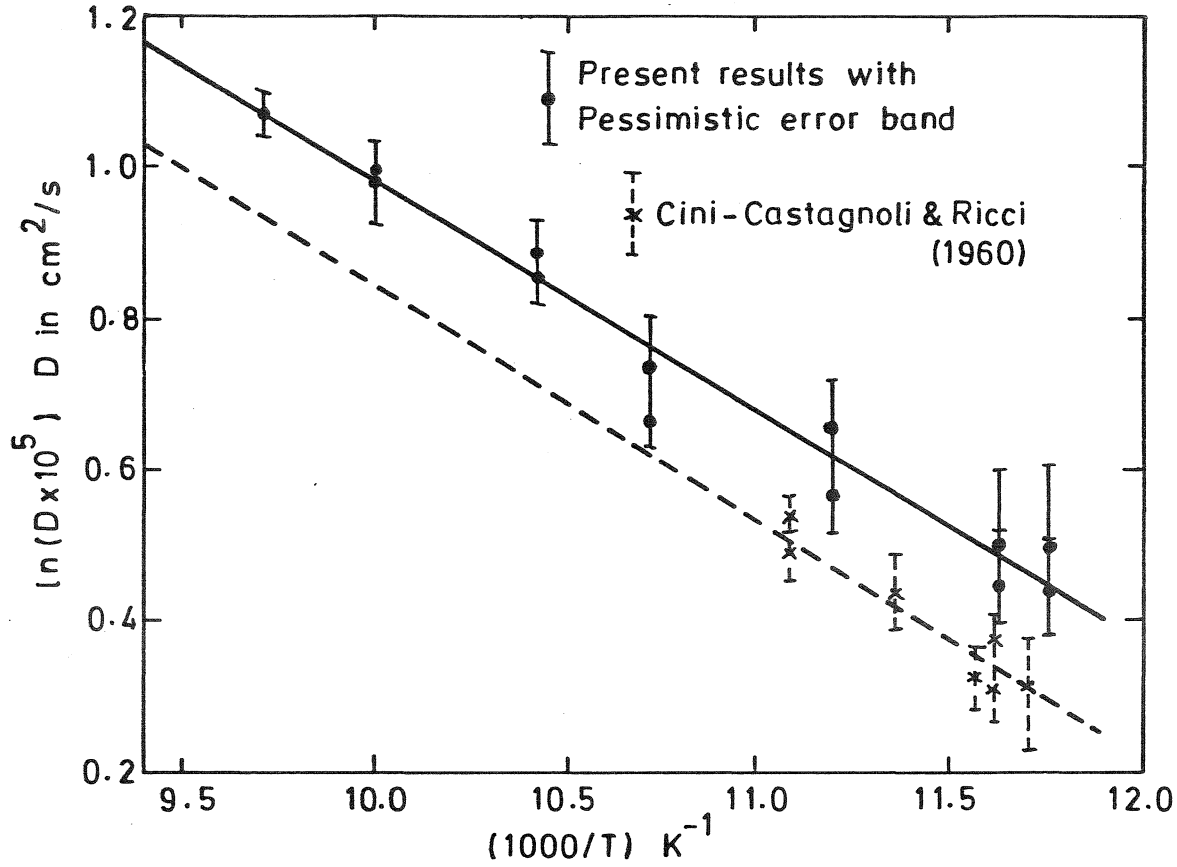

FIGURE 5.1 ARRHENIUS PLOT FOR D_{Kr}

6. DISCUSSION

The discussion of the results is presented in this chapter under the following headings: A) numerical accuracy, B) comparison with other experimental investigations and C) comparison with computer simulation results.

6.1 Numerical Accuracy

From a reference to Table 5.1 it can be observed that the uncertainty in the value of the diffusion coefficient varies between 1.5% and 7.8%. The uncertainty is caused by the following factors: a) the cell constant, b) the scatter in the value of 'b' of equation (3.5) in the mathematical processing and c) instability of the counting system. An uncertainty analysis is given in Appendix - II.

6.1.1 Uncertainty in the cell constant

The uncertainty in the cell constant was estimated to be 1%, which was due to ; i) uncertainty in the diffusion coefficient of the liquid used for calibration, ii) uncertainty in the contribution of the liquid lines to the actual volume of the cell, and iii) variation in the cell constant due to a change in temperature from the calibration to actual use conditions.

6.1.2 Uncertainty in the mathematical processing

The equation from which the diffusion coefficient was determined is equation (3.8). The value of index 'b' was obtained through a curve fit to the experimental data relating the counting rate and time. The criteria for least squares and the zeroes of the normal equations resulted in a scatter of the value of 'b'. In fact, the scatter itself was due to fluctuations in the counting system which was

also a source of uncertainty. Thus, a part of the instability in the counting system was already reflected in the scatter of 'b'. This uncertainty was found to be in the range of 0.4% to 3%.

6.1.3 Instability in the counting system

From an uncertainty analysis(given in Appendix - II) it can be seen that the uncertainty in 'b' is due to fluctuations in the counting rate ΔC and to a low value of the constant B, as given by the following equation:

$$\frac{\Delta b}{b} = - e \frac{\Delta C}{B} \quad . \quad (A2.7)$$

The magnitude of ΔC is dependent on the stability of the counting system. The fluctuations in the counting rate are about the same as the square root of the actual counts.

The value of the constant B can be increased by obtaining a high counting rate which is possible by introducing more tracer into the top compartment. This depends on the time allowed between breaking of the capsule and closing of the valve V_{T2} (Figure 4.2). This timing had to be optimised by trial and error. Consequently, in the initial stages of development it was not possible to standardize the filling procedure to obtain a high counting rate.

6.1.4 Repeatability

The precision of the apparatus can be gauged through repeatability of measured values. The worst case was at 89.3 K where it was as high as about 10%. The best consistency between two measurements was about 0.14% at 103 K.

6.1.5 Temperature

Platinum resistance thermometers were used for measuring and controlling temperatures. The resistance bridges used were accurate to 0.01 ohm which corresponds to about 0.023 K. There were no observable temperature gradients or time dependent fluctuations greater than 0.03 K. The thermocouples also indicated a flat profile for temperature of the cell. Thus, it can be confidently stated that the temperatures quoted in Table 5.1 are accurate to within 0.03 K.

6.1.6 Density

The pressures and temperatures at which the experiments were conducted (given in Table 5.1) were used to determine the densities from the tables published by Roder (1974). The pressures were measured with Bourdon type gauges which had a resolution of 2 psig (about 0.14 bar). The density variation was not more than 4.5×10^{-4} g/cm^3 per bar for liquid argon. Even if the uncertainty in pressure measurement was taken as 0.5 bar, the uncertainty in the value of density would be no more than 0.02%.

Considering the overall performance of the system after standardisation of its working, it is estimated that the smoothed diffusion data are accurate to within 3% and reproducible to within 3%.

6.2 Comparison with other Experimental Investigations

The tracer diffusion coefficients of krypton in liquid argon have been reported by only one set of investigators (Cini-Castagnoli and Ricci, 1960). The data covered a range of 85.4 to 90.2 K at a pressure of 2 atm. Capillary cell technique was used by those investigators.

6.2.1 Experimental technique

Temperature stability reported by Cini-Castagnoli and Ricci (1960) was ±0.05 K. Reproducibility of their apparatus could be gauged from a measurement at 90.2 K only which was 6%. The accuracy of their measurement was in the range of 2.3% to 7%.

The present diffusion cell was of the diaphragm cell type. It was designed to withstand a pressure of 500 bar. The light guide assembly was tested up to a pressure of 200 bar at room temperature and up to 100 bar at cryogenic temperatures. Using the same cell it is possible to span the entire liquid range of argon. Maximum temperature fluctuations were within ±0.03 K. The reproducibility was established at every temperature where diffusion coefficients were determined. It was found to vary from 0.14% to 9.5%. While these were the extreme limits, the average reproducibility was about 3%. Based on the uncertainty analysis the average error in measurement was estimated to be about 3%. The data obtained in this study cover a temperature range of 85 - 103 K.

6.2.2 Experimental results (Reference to Figure 5.1)

The activation energy for diffusion of krypton in liquid argon calculated from the present experiments and that of Cini-Castagnoli and Ricci (1960) differ by about 2.5%. However, the diffusion coefficients are found to differ by atleast 7%, the present values being consistently higher than those of the previous investigators. Considering the accuracies of the experimental techniques, there is a reasonable agreement between the two results as far as the magnitude of the diffusion coefficients are concerned.

6.3 Comparison with Molecular Dynamics Results

Although there are no theoretical predictions available for a system such as krypton in argon, it is of some interest to compare the present data with those obtained from computer simulation experiments. Of course, this comparison does not validate (nor invalidate) the experimental data, but at least indicates whether the molecular dynamics investigators are using a realistic model.

Jacucci and McDonald (1975) have obtained diffusion coefficients of krypton in argon-krypton mixtures as a function of mole-fraction of argon at about 116 K and a molar volume of 33.31 cm^3/mole. This corresponds to a pressure of about 11 bar which is not far from the conditions of the present experiments. These investigators observed that the diffusion coefficient of krypton in argon-krypton mixtures increases monotonically with mole fraction of argon. Figure 6.1 shows the variation as reported by them. In the present experiments the mole fraction of argon is almost unity. Using equation (5.1), which correlates the present data, the diffusion coefficient of krypton in argon at 115.7 K was extrapolated to be 4.02×10^{-5} cm^2/s. If the best fit data of Jacucci and McDonald (1975) is extrapolated to argon mole fraction of 1, the value of D_{Kr} can be found to be 4.0×10^{-5} cm^2/s. This agreement between the present data and the molecular dynamics calculations is fortuitous of course, but indicates that the computer simulation was based on a reasonable model.

According to equation (5.2) which represents the results obtained by Cini-Castagnoli and Ricci (1960), D_{Kr} was found to be 3.54×10^{-5} cm^2/s. This value is lower than the computer simulation result by about 13%. But, considering the fact that the data of Cini-Castagnoli and Ricci (1960)were extrapolated far from the region of

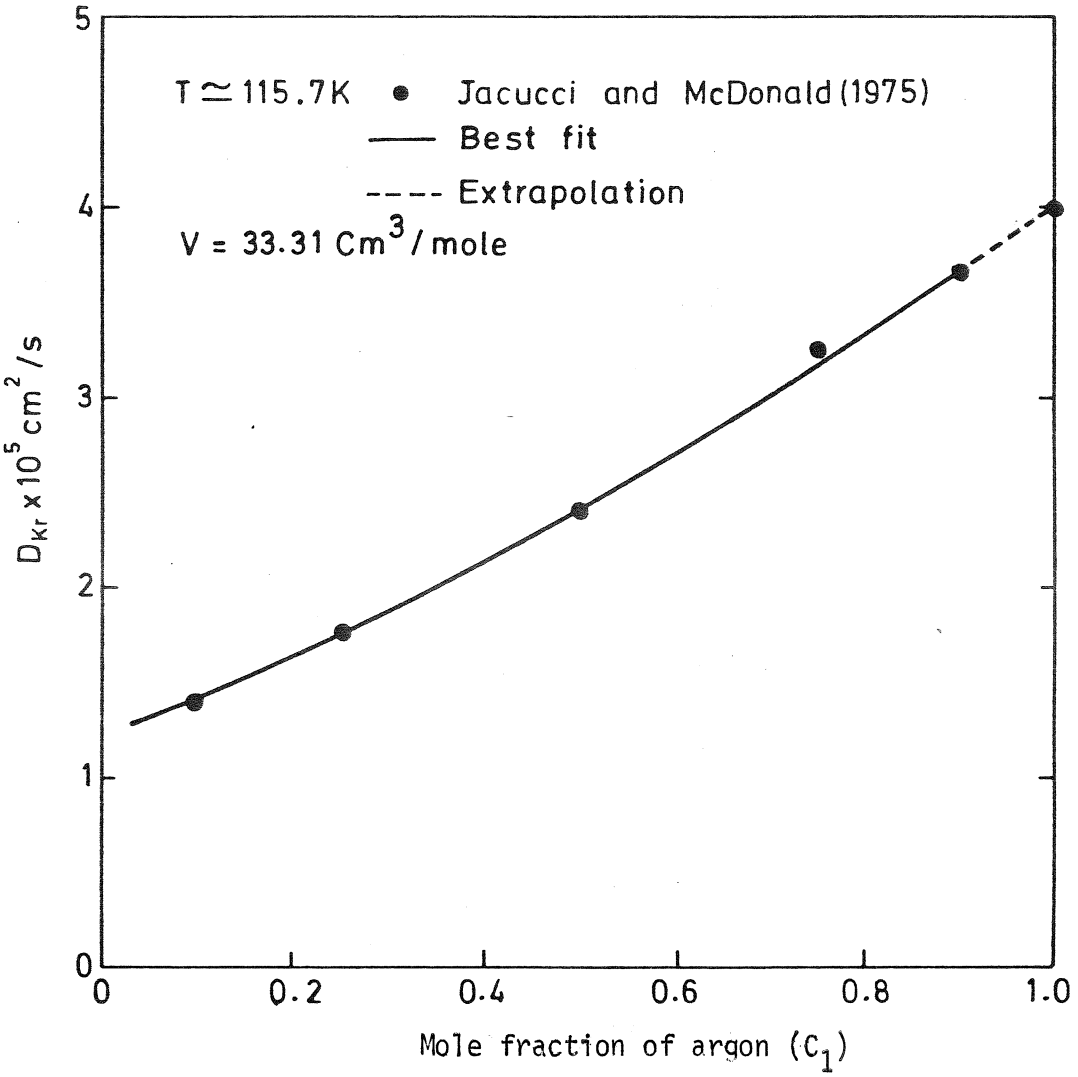

FIGURE 6.1 VARIATION OF D_{Kr} WITH C_1 IN ARGON-KRYPTON MIXTURES AT ABOUT 115.7 K

their experiments such a deviation is not unexpected.

With certain evidence and assumptions, argon self-diffusion coefficient can be estimated using the present data and the results of computer simulation. However, one should await actual experimental data on argon self-diffusion before deriving any positive conclusions.

7. SUGGESTIONS FOR FUTURE WORK

The present experimental facility can be used to obtain more diffusion data. The suggested direction for future work is based on the following: a) extension of range of krypton tracer diffusion, b) self-diffusion of argon, c) self-diffusion of krypton and d) diffusion experiments under pressure.

7.1 Extension of Range of Krypton Tracer Diffusion

Experiments can be conducted up to the critical temperature of argon. The pressure needed is less than 50 bar. To operate at temperatures higher than 103 K, the copper vessel needs to be insulated . Polystyrene foam is suggested. The thickness of lagging can be calculated by solving the heat conduction equation for the compound cylinder of insulation and the copper vessel.

7.2 Self-diffusion in Liquid Argon

During the present study, efforts were made to obtain self-diffusion data for liquid argon using Ar^{37} as the tracer. In the opinion of the author, it is unlikely that the present system of continuous monitoring would respond to the radiation emitted by Ar^{37}. Either a highly sensitive X-ray detector dipped well into the top compartment and well shielded from the magnetic field has to be used or the tracer should be substituted by either Ar^{39} or Ar^{42}. Unfortunately, none of these isotopes are commercially available, yet.

7.3 Self-diffusion in Krypton

To obtain self-diffusion data for liquid krypton the cell has to be operated at a temperature above 116 K with suitable modifications to the condensing system. Cryopumping of krypton into the

cell is suggested. Suitable gas recovery system has to be designed since krypton is a very expensive gas.

There is a great demand for reliable and confirmatory data on self-diffusion in liquids argon and krypton and it is hoped that the present apparatus provides a scope for obtaining them.

7.4 Diffusion Experiments under Pressure

Present experiments covered a temperature range of 85 - 103 K, but the pressures were close to atmospheric. However, theorists would appreciate results for the density dependence of the diffusion coefficients. The cell has been designed to withstand a pressure of 500 bar and the light guide can be used up to a pressure of 200 bar. At higher pressures a stainless steel clad lucite light guide is suggested.

To increase the pressure, the property of volumetric expansion of the liquid can be utilised. The cell may be isolated at a pressure lower than the one required and then warmed up to increase the pressure. Pressure monitoring in such case should be done with carbon resistors or pressure sensitive crystals or calibrated manganin wires.

8. CONCLUSIONS

The contribution of the present study has been to design and develop an experimental facility for diffusion studies on cryogenic liquids. Tracer diffusion data for krypton in liquid argon have been obtained in the temperature range of 85 - 103 K and pressures close to atmospheric. The following conclusions are derived from the present study:

1. the diaphragm cell method, which has been used to obtain accurate diffusion data at room temperatures, can also be adapted for measurements at cryogenic temperatures,

2. the scintillation counting system is appropriate for studying diffusion of radioactive krypton as tracer in liquid argon,

3. the continuous gas flow method of temperature control is capable of giving a good temperature stability with the fluctuations being within ± 0.03 K over a period of several days, and

4. the tracer diffusion data is accurate to 3% and reproducible to 3%.

REFERENCES

Blancett A.L and Canfield F.B (1966), Adv. Cryo. Eng., 11,612

Buckingham R.A (1957),"Numerical Methods", Sir Issac Pitman and Sons Ltd., London

Cini-Castagnoli G and Ricci F.P (1960), Il Nuovo Cimento,XV, No.5,795

Collings A.F and Mills R (1973), Trans. Faraday Soc.,66, Part II,2761

Corbett J.W and Wang J.H (1956), J. Chem. Phys., 25, 422

Cowgill D.F and Norberg R.E (1976), Phys. Rev.,13,2773

Dasannacharya B.A and Rao K.R (1965), Phys. Rev.,137,417

Fenyves E and Haiman O (1969),"The Physical Principles of Nuclear Radiation Measurements", Academic Press, New York

Friedlander G and Kennedy J.W (1949), "Introduction to Radiochemistry" John Wiley and Sons ,New York

Godwin R.D (1960), Adv.Cryo.Eng.,4, 487

Hansen J.P and McDonald I.R (1976), "Theory of Simple Liquids", Academic Press, London

Jacucci G and McDonald I.R (1975), Physica, 80A,607

Kemp R.G (1977), "International Practical Temperature Scale of 1968 (Amended Edition, 1975)", National Measurement Laboratory, CSIRO, Lindfield, NSW

Kline S.J and McLintock F.A (1953), Mech. Eng.,75, 3

Kubota S, Masahiko H and Akira N (1978), Nuclear Instrum. & Methods,150,561

McCool M.A (1971), "Diffusion in Organic Liquids: Pressure, Temperature Studies", Ph.D thesis, The Australian National University

Mills R (1961), Rev. Pure Appl. Chem.,11,78

Mills R (1973), J. Phys. Chem.,77,685

Mills R (1974), "Molecular Motions in Liquids", Ed. Lascombe J, D.Reidel Publishing Co.,Dordrecht, Holland, 391

Mills R and Woolf L.A (1968), The diaphragm Cell, DRU-RR-1, The Australian National University Press, Canberra

Mott N.F (1952), Proc. Royal Soc.,A-215,1

Naghizadeh J.N and Rice S.A (1962),J. Chem. Phys.,36,2710

Pryde J.A (1966)," The Liquid State", Hutchinson University Library, London

Roder H.M (1974)," Liquid Densities of Oxygen, Nitrogen, Argon and Para-hydrogen", NBS Tech. Note 361 (Revised) - Metric Supplement, U.S Dept. of Commerce, Washington

Stokes R.H (1950), J.Am. Chem. Soc.,72,763

Van Loef J.J (1972), Physica, 62,345

Watts R.O and McGee I.J (1976)," Liquid State Chemical Physics", John Wiley and Sons, New York

Wigley D.A and Halford P (1971), Chapter 6 in "Cryogenic Fundamentals", Ed. Haselden G.G , Academic Press, London

Zandveld P, Andriess C.D, Bregman J.D, Hasman A and Van Loef J.J (1970), Physica, 50, 511

APPENDIX - I

Details of the Method of Curve Fitting

Equation (3.5) is a difficult curve to fit because of the constant A. In its absence it would have been straight forward to fit an exponential curve.

If C_{T_i} (i=1,N) are the counts corresponding to t_i (i=1,N) the value of A cannot exceed the lowest value of C_T which is when i=N. In fact, the value of A is only the value of C_T as $t \to \infty$. Thus, it is possible to guess the range of the value of A in equation (3.5). The least squares fit can then be carried out for different values of A around the guessed value.

Let C_i' be the correct value of counting rate at t_i, and e_i be the difference between the actual counting rate and smoothed counting rate. Consequently,

$$e_i = (C_{T_i} - C_i') \quad . \quad (A1.1)$$

For least squares, the sum of the squares of deviations between the measured and smoothed counting rates should be a minimum. The sum of the squares of deviations can be represented as follows:

$$E = \Sigma e_i^2 = \Sigma (C_{T_i} - C_i')^2 \quad * \quad . \quad (A1.2)$$

But,

$$C_i' = A + B \exp (-b\, t_i) \quad . \quad (A1.3)$$

Therefore, equation (A1.2) can be written as follows:

$$E = \Sigma [C_{T_i} - A - B \exp (-bt_i)]^2 . \quad (A1.4)$$

---

* All summations are from i= 1,N

Since there are three parameters (A, B and b), to minimise the sum of the squares of the deviations the following conditions are necessary:

$$\frac{\partial E}{\partial A} = \frac{\partial E}{\partial B} = \frac{\partial E}{\partial b} = 0 \qquad \text{. (A1.5)}$$

Using the equations (A1.4) and (A1.5) the normal equations can be written as below:

$$\Sigma \quad [\, C_{T_i} - A - B \exp(-bt_i) \,] = 0 \quad \text{, (A1.6)}$$

$$\Sigma \quad [\, C_{T_i} - A - B \exp(-bt_i) \,] \exp(-bt_i) = 0 \quad \text{, (A1.7)}$$

and

$$\Sigma \quad [\, C_{T_i} - A - B \exp(-bt_i) \,] \exp(-bt_i)\, t_i = 0 \quad \text{. (A1.8)}$$

The normal equations have their own significance:

a) equation (A1.6) yields a condition that the sum of the deviations should be zero,

b) equation (A1.7) provides a condition that the sum of the weighted deviations should be zero. In radioactive counting the standard deviation is proportional to the square root of the counting rate (Friedlander and Kennedy,1949). For a top-loaded run, the counting rate at the beginning of an experiment is higher than that at the end. Hence, it is appropriate that the deviations be weighted. Since the equation (A1.7) automatically provides the necessary weighting factor through the exp $(-bt_i)$ term, no other weighting factors were used, and

c) equation (A1.8) compensates for the over weighting . It provides a condition that the sum of the areas formed by the weighted deviations and the time at that instant be zero. Equation (A1.7) weights the values of C_{T_i} at the beginning of an experiment higher than those at the end, whereas equation (A1.8) does the contrary.

In the above analysis it is assumed that the uncertainty in the measurement of time is negligible. This is reasonable because the counting was actuated and stopped by high precision electronic timers which are accurate to better than 1 part in 10^4. Counts were taken for one minute followed by a dwell time of one minute. Six sets of consecutive counts were averaged and the resulting counting rate was taken to be the one corresponding to the time at the beginning of the set.

The flow chart for the computation scheme is shown in Figure A1.1. When the value of A has been guessed, equation (3.5) can be written as follows:

$$y = B \exp(-bt_i) \quad , \text{(A1.9)}$$

where

$$y = C - A \quad^{*} \quad . \text{(A1.10)}$$

Since the values of (t_i, y_i) are known at N points, the parameters b and B can be computed using the following relations:

$$-b = \frac{\Sigma (t_i \ln y_i) - \frac{1}{N} (\Sigma t_i)(\Sigma \ln y_i)}{\Sigma t_i^2 - \frac{1}{N} (\Sigma t_i)^2} \quad , \text{(A1.11)}$$

and

$$B = \exp\left[\frac{\Sigma \ln y_i}{N} + b \frac{\Sigma t_i}{N}\right] \quad . \text{(A1.12)}$$

In an ideal least squares fit problem all the four criteria, namely the ones described by equations(A1.4) and (A1.6) to (A1.8) will be satisfied simultaneously. However, it may not happen in a real situation due to inherent fluctuations in counting rate.

---

* C and C_T are synonimous.

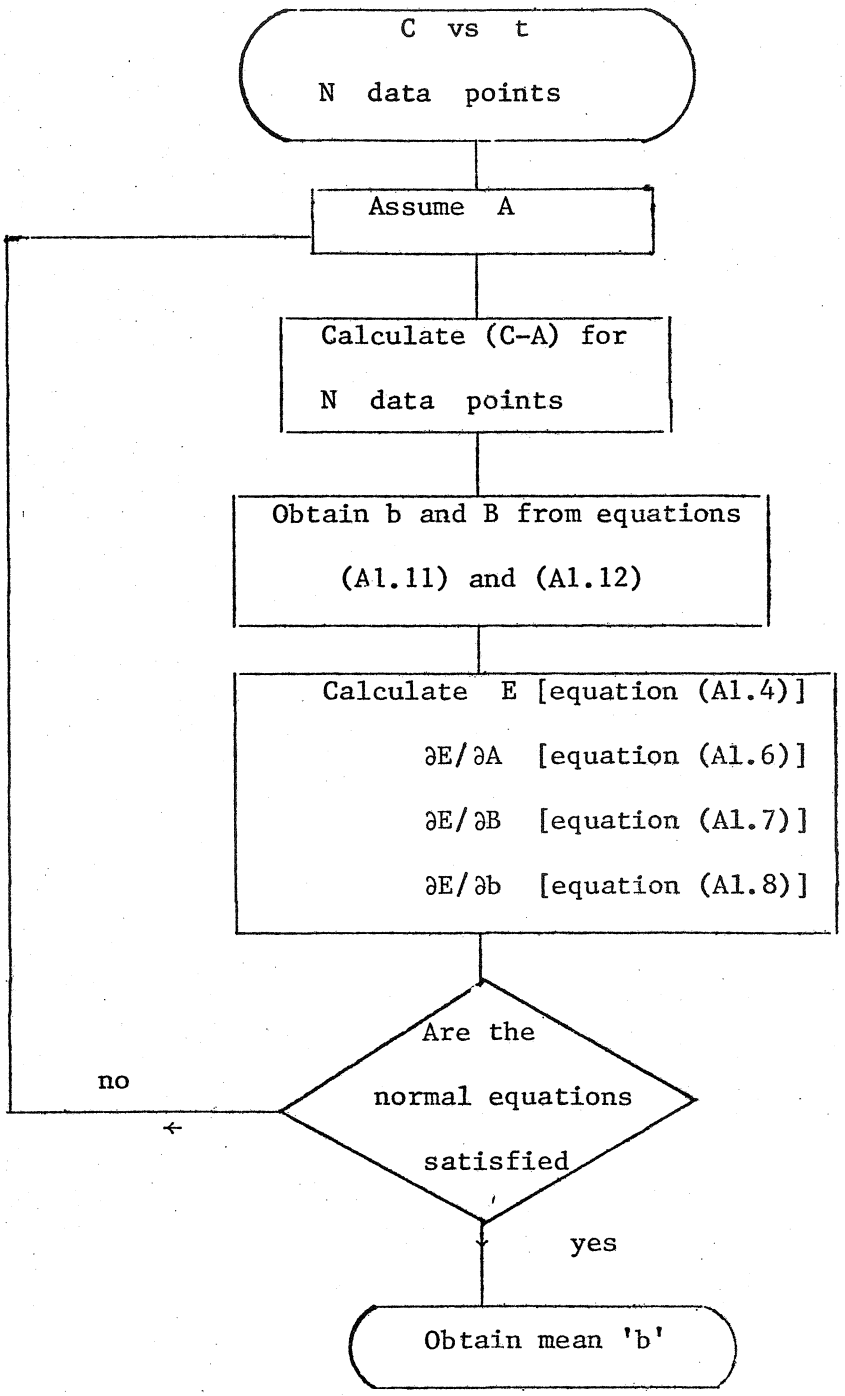

FIGURE A 1.1 : FLOW CHART FOR THE CALCULATION SCHEME

APPENDIX - II

Uncertainty Analysis

The diffusion coefficient is determined from the following equation:

$$D = \frac{b}{\beta} \qquad . \quad (A2.1)$$

The error equation can be obtained by expressing the above equation in the differential form as follows:

$$\frac{\Delta D}{D} = \frac{\Delta b}{b} - \frac{\Delta \beta}{\beta} \qquad . \quad (A2.2)$$

It has been estimated (Section 4.1.1) that the uncertainty in the cell constant is ± 1% (ie., $\Delta\beta/\beta$).

Determination of $\Delta b/b$

$\Delta b/b$ can be obtained from the following equation:

$$C = A + B \exp(-b\ t) \qquad . \quad (3.5)$$

By differentiating the above equation the following error equation can be obtained:

$$\Delta b = \frac{\exp(bt)}{B\ t} [\ \Delta A + \Delta B \exp(-bt) - \Delta C\ ] \qquad . \quad (A2.3)$$

ΔA and ΔB can be determined by the curve fitting method described in the Appendix - I. The computational accuracy attainable is 1 part in 30000. The maximum contribution is through ΔC which is due to fluctuations in the counting rate. These are induced by drifts in the amplifier gain and disciminator settings and instability in the high voltage power supply of the photomultiplier tube. The range of ΔC is up to 200 counts/min. This is also the precision of the counting system. Equation (A2.3) can be approximated as follows:

$$\Delta b = -\frac{\Delta C \exp(bt)}{B\ t} \qquad . \quad (A2.4)$$

The error in b is a minimum for a given 't' which can be obtained by differentiating the above equation w.r.t. 't' and solving for 't' when the differential is equal to zero. The resulting equation is given below:

$$\frac{\partial}{\partial t}(\Delta b) = -\frac{\Delta C \exp(bt)}{B\,t}\left(\frac{1}{t} - b\right) = 0 \quad , \qquad (A2.5)$$

which yields the condition that

$$t = 1/b \quad . \qquad (A2.6)$$

Substituting equation (A2.6) in (A2.4) one obtains

$$\frac{\Delta b}{b} = -\,e\,\frac{\Delta C}{B} \quad . \qquad (A2\ 7)$$

In the above equation ΔC can be obtained from the standard deviation of the counting rate. The relation is

$$\Delta C = \sqrt{[E/(N-1)]} \quad , \qquad (A2.8)$$

where E is defined by equation (A1.4) and N is the number of data points.

The Kline and McLintock (1953) method can be used to predict the overall uncertainty. Here the scatter in the mathematical value of 'b' (due to equations (A1.4) and (A1.6) to (A1.8) of Appendix - I) is also added to give a pessimistic error band. Consequently,

$$\frac{\Delta D}{D} = \sqrt{\left[\left(\frac{e\,\Delta C}{B}\right)^2 + \left(\frac{\Delta \beta}{\beta}\right)^2 + (\text{Scatter in 'b'})^2\right]} \quad . \qquad (A2.9)$$

A case study is presented in the next Appendix.

APPENDIX - III

A Case Study of Data Analysis

Diffusion experiment at 103 K (Run Id : NOV12) is analysed here to explain the sequence of data processing.

The starting time for diffusion experiment was reckoned 18 hours after the introduction of tracer into the top compartment. However, diffusion would have occured during this period. For this reason $^{o}C_{B} \neq 0$. The data available were in the form of a typewriter output at six sets of counts per line which covered a period of 12 min. Counts on each line were averaged and the resulting count rate was assumed to correspond to the time of the first count. The count rate (C) and time (t) from the arbitrary starting time were fed into a data file. All the computations were done on a DEC 10 computer.

Equation (3.5) gives the type of curve to be fitted. The flow chart for the computation scheme is given in Figure A1.1. In the actual computer program the iteration was performed by feeding a guess value of 'A' in separate computations. This was found to be advantageous as the best fit for the parameters A, B and b could be obtained in 8 to 10 iterations. Rapid turn around through interactive terminals enabled this procedure.

Figure A3.1 (a) shows the plot of actual counting rate as a function of time. Figure A3.1 (b) shows a plot of ln(C-A) vs t. The latter plot will be obviously linear. It may be noted that the instant t=0 is different for the two figures. In the latter, it is the beginning of the zone of computation from Figure A3.1 (a). The following Table gives the details of the experiment:

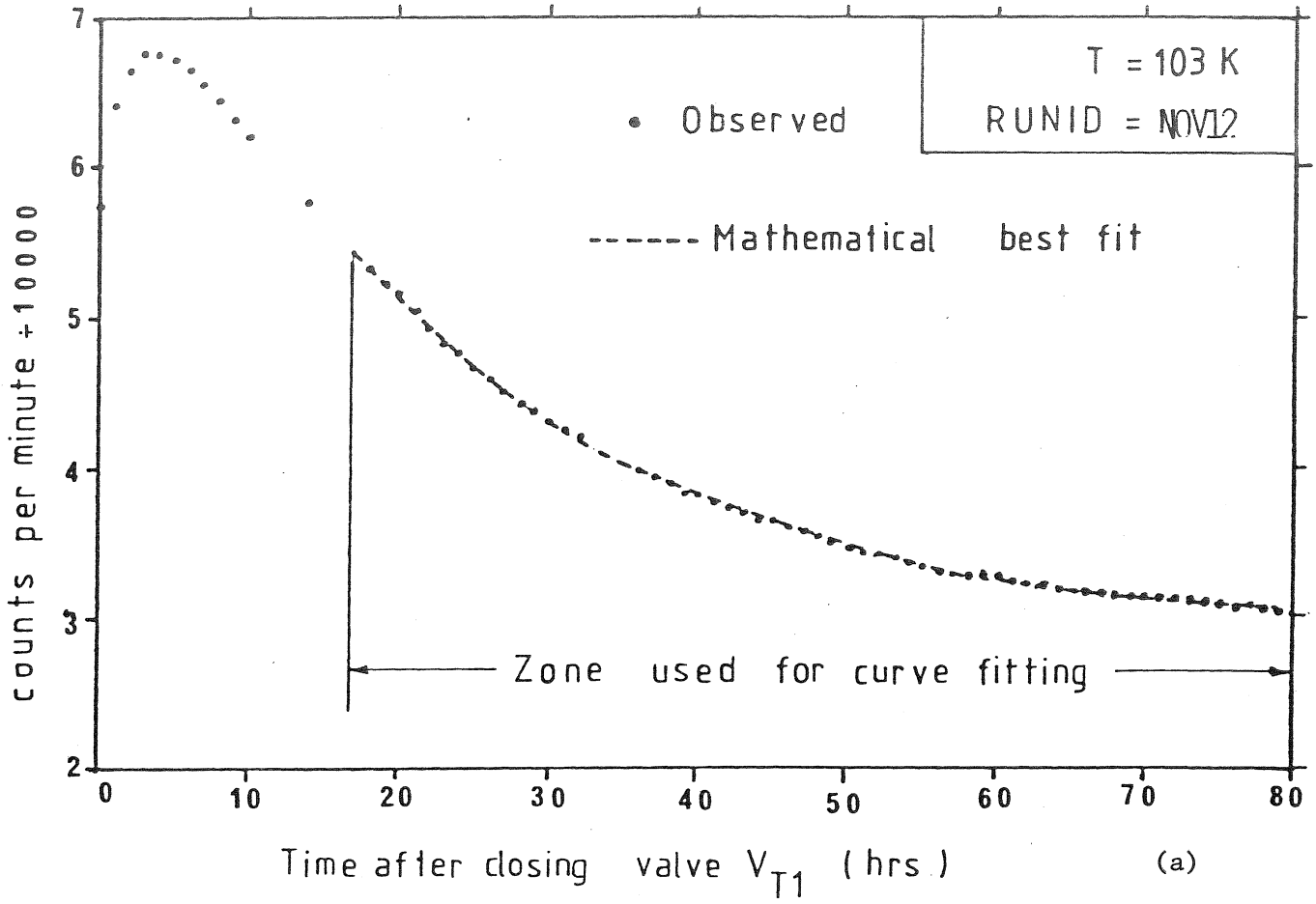

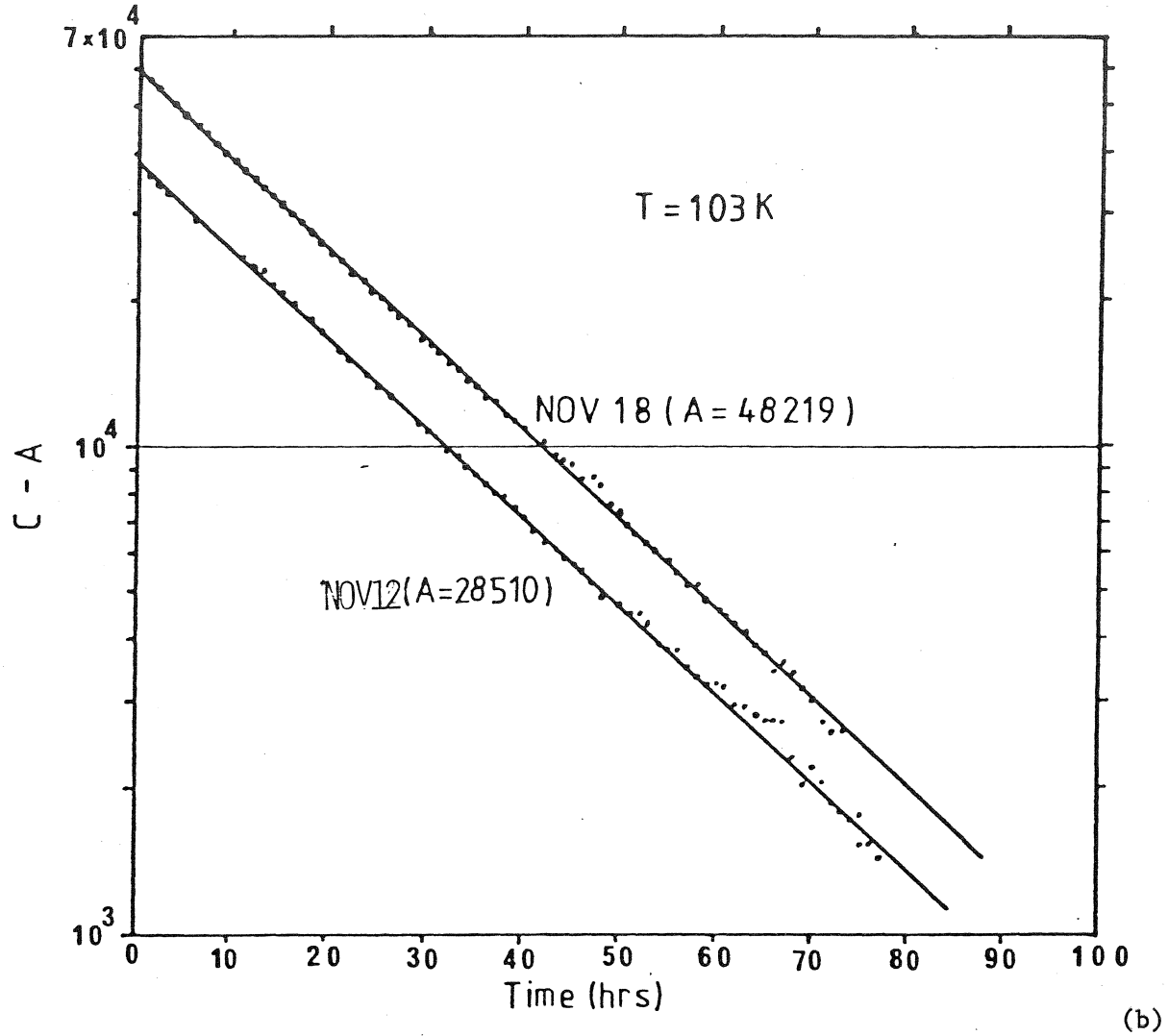

FIGURE A3.1 : VARIATION OF COUNT RATE DUE TO DIFFUSION

TABLE A3.1 : DETAILS OF DIFFUSION EXPERIMENT AT 103 K (Run ID: NOV12)

Temperature	:	103 K
Pressure	:	4.8 bar
Density of liquid argon:		1.2911 g/cm^3
No. of data points	:	492
Starting time for computation after closing the valve V_{T1}	:	18 hrs
Total duration of experiment	:	80 hrs

Critria used	A	B	b x 10^4 (min^{-1})
E = minimum	28515	39308	7.05058
$\partial E/\partial A = 0$	28521	39459	7.07170
$\partial E/\partial B = 0$	28510	39185	7.03316
$\partial E/\partial b = 0$	28504	39039	7.01246

Standard deviation	:	196 counts/min
Correlation coefficient	:	98.9%
Average value of 'b'	:	7.042 x 10^{-4} min^{-1}
Cell constant	:	0.4023 cm^{-2}
Diffusion coefficient	:	2.917 x 10^{-5} cm^2/s

Because the curve fitting problem is based on a non-linear least squares method, the values of A, B and b are not unique. Such a discrepency is very common with fits which are sums of exponential functions (Buckingham, 1957). Physical realism necessitates that 'b' be of the order of 10^{-5} s^{-1}. In the process of curve fitting a search is made for a local minimum in the least squares.

Estimation of uncertainty

From the Appendix - II, the uncertainty in the value of 'b' is given by:

$$\left|\frac{\Delta b}{b}\right| = e\,\frac{\Delta C}{B}$$

Here ΔC is 196 counts/min , B is 39248 counts/min . Hence, $\Delta b/b \simeq 1.4\%$. However, there is a scatter of about 0.4% in the value of 'b' itself. Using the method of Kline and McLintock (1953) the overall uncertainty can be estimated as follows:

$$\frac{\Delta D}{D} = \sqrt{\left|\frac{\Delta b}{b}\right|^2 + \left|\frac{\Delta \beta}{\beta}\right|^2 + \left|\text{scatter in 'b'}\right|^2}$$

$$= [\,1.4^2 + 1^2 + 0.4^2\,]^{\frac{1}{2}} \quad \%$$

$$= 1.7\%$$

However, the effect of fluctuations in the counting system is reflected in both $\Delta b/b$ and the scatter of 'b'. Thus, the above estimate is a pessimistic one.

Reproducibility

At 103 K another experiment yielded a result of $2.921 \times 10^{-5}\ cm^2/s$ for D_{Kr}. In this case the results agree within 5 parts in 3000.